Nanometer scale carbon structures for charge-transfer systems and photovoltaic applications

Dirk M. Guldi

Received 4th December 2006, Accepted 3rd January 2007
First published as an Advance Article on the web 8th February 2007
DOI: 10.1039/b617684b

This article surveys and highlights the integration of *nanometer scale carbon structures*—in combination with chromophores that exhibit (i) significant absorption cross section throughout the visible part of the solar spectrum and (ii) good electron donating power—into novel electron donor–acceptor conjugates (*i.e.*, covalent) and hybrids (*i.e.*, non-covalent). The focus of this article is predominantly on performance features—charge-transfer and photovoltaic—of the most promising solar energy conversion systems. Besides documenting fundamental advantages as they emerge around *nanometer scale carbon structures*, critical evaluations of the most recent developments in the fields are provided.

Introduction

It is foreseeable that artificial photosynthetic systems that will ultimately power practical solar fuels production must be based on molecular and supramolecular assemblies.[1] Specific requirements that such assemblies must meet include the collection of light energy, separation of charges, and transport of charges to catalytic sites, where water oxidation and CO_2 reduction will occur. Notable progress has been made on each aspect of these complex problems—yet researchers have not developed components that are both efficient and robust, and have not integrated the existing functional components into a working system.[2] The design and development of light harvesting, photoconversion, and—as a long term aim—catalytic modules capable of self-ordering and self-assembling into an integrated functional unit will make it possible to realize efficient artificial photosynthetic systems based on nanometer scale carbon structures.

Electron acceptors

A first prominent example of nanometer scale carbon structures are fullerenes—see Scheme 1. Ever since their initial discovery, scientists worldwide have studied their solid state properties ranging from superconductivity and nanostructured devices to endohedral fullerene chemistry.[3] Hereby, the three-dimensional structure of fullerenes, which exclusively consist of electron-rich hexagons and electron-deficient pentagons, evoked a lively interest to relate their properties to conventional one-dimensional π-systems. The extraordinary electron acceptor properties of, for example, the most abundant fullerene, namely, C_{60} with a diameter of 7.8 Å, have led to noteworthy utilizations of such nanoscale architectures in areas of light-induced electron transfer chemistry and solar energy conversion.

Importantly, original and well-established synthetic methodologies emerged as potent means en-route to a wide variety of novel fullerene derivatives.[4] Such methodologies ensure the complete control over chemically functionalizing fullerenes in simple or even sophisticated ways. With these methods in hand, the synthesis of relatively complex molecular tectons—one-dimensional, linear arrays and three-dimensional, spheroidal architectures—has been accomplished. In these tectons the unique electrochemical and photophysical features, which pristine C_{60} exhibits, have largely been preserved.

More recently, a different class of nanometer scale carbon structures is drawing considerable attention: carbon nanotubes (CNT)—see Scheme 1.[5] Of the wide range of CNT, single wall carbon nanotubes (SWNT) protrude as unique materials: they are fascinating, with exceptionally high tensile

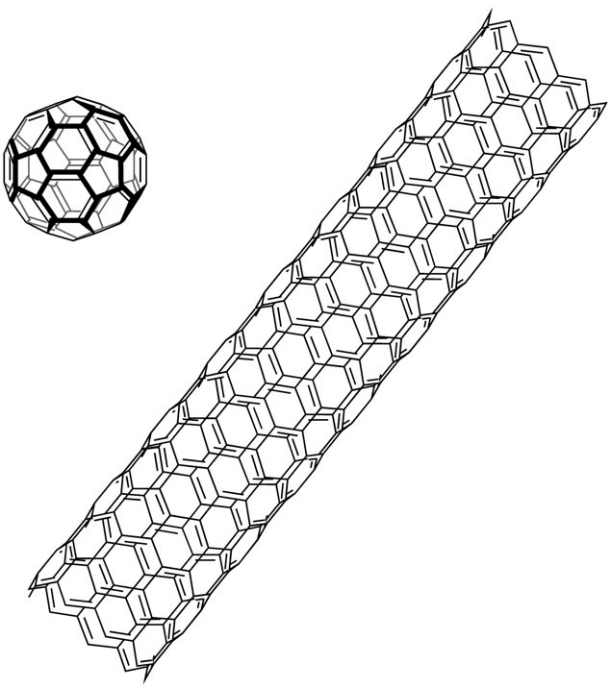

Scheme 1 Molecular building blocks—C_{60} and single wall carbon nanotubes (SWNT)—as electron acceptors.

Universität Erlangen, Institute of Physical and Theoretical Chemistry, 91058 Erlangen, Germany

strength, the highest thermal conductivity known and extraordinary field emission properties.

In contrast to fullerenes, SWNT are one-dimensional nanometer scale carbon structures.[5] Structurally, CNT are a member of the fullerene family. However, in contrast to the spherical nature of fullerenes, CNT are cylindrical, with at least one end typically capped with a fullerene hemisphere. The structure of a SWNT can be conceptualized by wrapping a one-atom-thick layer of a graphene sheet, that is, an interlinked hexagonal lattice of carbon atoms, into a seamless cylinder. The way the graphene sheet is wrapped is represented by a pair of indices (*n*,*m*) called the chiral vector. The diameter of most SWNT is close to 1 nm, with a tube length that might be many thousands of times larger. For instance, SWNT with lengths up to several centimetres have been produced to yield impressively high aspect ratios.

MWNT consist of multiple layers of graphite rolled in on themselves to form a tube shape. They are constructed by rolling several cylinders of graphene sheets, each cylinder with a slightly larger circumference then the first.[6]

The technological interests in CNT rest on their exceptional mechanical, electrical and optoelectronic properties.[5] CNT materials show much improved features relative to classical materials like organic polymers or semiconductors. Some nanotubes are, for example, stronger than steel, lighter than aluminium and more conductive than copper or silver. All of these remarkable properties give CNT a range of potential applications: for example, in reinforced composites, sensors, nanoelectronics and display devices. Moreover, the graphitic surface of SWNT is chemically very robust, which, in turn, guarantees long-term stable operations.

Important breakthroughs—prompting the potential use of CNT in controlling other nanoscale structures—have already been achieved in fields like electronics, optoelectronics, sensors, fillers in new generation polymer composites, therapeutics and diagnostics.[7] Most of the aforementioned applications implement electron transfer reactions that evolve between CNT and photo- and electroactive materials. The high polarizability and the smooth surface of SWNT is the inception of strong van der Waals interactions, reaching values as high as 500 eV per 1 μm of CNT length, and to aggregation into insoluble bundles and/or ropes.[8] Such features are responsible for the low solubility of SWNT in common organic solvents. Important for the chemical reactivity is the fact that metallic CNT are slightly less aromatic than semiconducting ones and, in turn, more reactive than the latter.

Fullerenes and CNT are natural electron acceptors.[9] Qualitative molecular orbital theory follows isolated C_2 fragments that are brought together starting from infinite distance. Implicit is that each C_2 fragment possesses a π and a π* orbital. If these fragments are brought together—forming, for example, a SWNT—the two degenerate sets of π and π* orbitals mix. Energetically, they spread, with the low-lying edge of the π* orbitals ready to accept electrons. In the context of charge-transfer, an additional attribute of CNT should be considered. In particular, all nanotubes are expected to be very good thermal conductors along the tube, exhibiting a property known as "ballistic conduction". Note, however, that CNT are good insulators laterally to the tube axis. Thus, CNT not only act as electron acceptors but also provide high fields at the donor/CNT interfaces for exciton dissociation.

Electron donors: chromophores

In light of the moderate absorption features of the aforementioned nanometer scale carbon structures in the visible range, functionalization with chromophoric functionalities has developed as an important objective. Leading examples are gathered in Scheme 2. Such an approach is meant to promote the visible absorption characteristics of the resulting conjugates/hybrids and, importantly, to improve the light harvesting efficiency. Specifically, suitable photosensitizers assist to extend the absorption further into the red, yielding, upon excitation, energetically low-lying excited states. As a direct consequence, the role of the nanometer scale carbon structures is significantly changed. Under these circumstances, *i.e.*, bearing a photoactive and electroactive moiety, nanometer scale carbon structures operate nearly exclusively as electron and/or energy acceptor moieties.

Porphyrinoid and especially metalloporphyrinoid systems—with their rich and extensive absorptions throughout the visible region of the solar spectrum—hold particularly great promise as integrative building blocks with increased absorptive cross sections.[10] Over the course of recent years

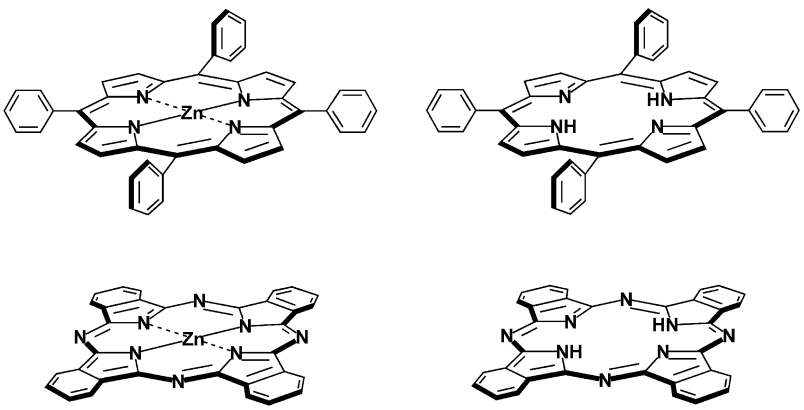

Scheme 2 Molecular building blocks—porphyrins (*i.e.*, ZnP and H_2P) and phthalocyanines (*i.e.*, ZnPc and H_2Pc)—as chromophores and electron donors.

they emanate as light harvesting building blocks in the construction of molecular architectures. Their high electronic excitation energy, typically exceeding 2.0 eV, powers a strongly exergonic electron transfer and intercedes hereby the conversion between light and chemical/electrical energy. Another important feature of porphyrins is their highly delocalized π-electron systems. Such delocalization results—upon an uptake or release of electrons—in minimal structural change upon electron transfer. Rich redox properties render porphyrins and porphyrin analogues as essential components in important biological electron transport systems including photosynthesis and respiration.

Another class of chromophoric functionalities is phthalocyanines.[10] They play a central role in view of their outstanding electronic properties, which rely on their extensive aromatic π-system. These planar macrocycles are ideally suited for photovoltaic applications, since they present exceptional optical and thermal stability, strong absorption in the visible, finely tunable redox properties, and may be incorporated into different kinds of condensed phases, due to their tendency to aggregate by π–π stacking. Most importantly, the strong absorption of phthalocyanines in the solar spectrum with extinction coefficients as high as 200 000 M^{-1} cm^{-1} in the 700 nm range, together with their rich redox chemistry, provides both excellent light harvesting and electron donor features and hints at their potential. Phthalocyanines can also function as electron acceptors, which depends, in part, on the peripheral substitution and the corresponding counterpartner.

General aspects of charge-transfer systems

The Marcus theory of electron transfer, which treats the rate constants of non-adiabatic intramolecular electron transfer—for both charge separation (k_{CS}) and charge recombination (k_{CR}) —as a parabolic dependence on the free energy changes of the reaction ($-\Delta G^{\circ}_{CS}$ or $-\Delta G^{\circ}_{CR}$).[11] This relationship provides a valuable guide for the control over the efficiency and kinetics of charge separation *versus* charge recombination. The electronic coupling (V) between donor and acceptor states and, foremost, the reorganization energies (λ) regulate the absolute rate constants.

Notably, the rate constant first increases with increasing thermodynamic driving force ($-\Delta G^{\circ} < \lambda$). This range is generally referred to as the Marcus *normal* region of the bell-shape relationship. When the driving force becomes, however, of the same magnitude as the reorganization energy ($-\Delta G^{\circ} \sim \lambda$), the reaction rate reaches a maximum. Under such conditions, the rate constant is basically controlled by the magnitude of electronic coupling (V) between the interacting donor and acceptor moieties. Hereby, V relates to the overlap of the donor and acceptor orbitals. Upon passing the thermodynamic maximum ($-\Delta G^{\circ} \sim \lambda$), the highly exothermic region of the parabola ($-\Delta G^{\circ} > \lambda$) is entered. Here, an additional increase of the free energy change results in an actual slow down of the reaction rate. An increasingly poor vibrational overlap of the product and reactant wavefunctions, is responsible for this behavior. The highly exergonic range is generally referred to as the Marcus *inverted* region.

The ultimate goal of any solar energy conversion system should be to power a thermodynamically driven charge separation event to yield a highly energetic radical ion pair. Perceptibly, charge separation should take place at small free energy changes, $-\Delta G^{\circ}_{CS}$. This is beneficial, to store most of the excited state energy. Just the contrary consideration holds for the energy gap that characterizes the charge recombination ($-\Delta G^{\circ}_{CR}$): this should be kept as large as is feasible. Ideally, large energy gaps should ensure dynamics that are deeply shifted into the Marcus *inverted* region and, consequently, to slow down the limiting and energy wasting charge recombination.

In the context of modulating the electron transfer rates, variation of the reorganization energy (λ) is an effective way. In particular, modifying λ influences the maximum of the parabolic log k_{ET} *versus* $-\Delta G^{\circ}_{ET}$ dependence on the abscissa. A closer look reveals even more dramatic impacts on the activation energies for the charge separation ($\Delta G^{\#}_{CS}$) and the charge recombination ($\Delta G^{\#}_{CR}$). These are much reduced and increased, respectively, when λ gets smaller. An ideal scenario implies small reorganization energies. Fig. 1 illustrates this explanatory for a spherical C_{60} and a planar naphthalenediimide. This leads to optimal charge-separation kinetics, which are located near the top of the Marcus curve—even if the driving forces are small—and a deceleration of the charge recombination rates, which are buried far into the Marcus *inverted* region.

This raises the crucial question: what would determine a small λ and especially what would render nanometer scale carbon structures particularly promising acceptor candidates. The energy required to reorganize any given system to an optimum configuration for electron transfer defines λ. Before going into structural details, it should be noted that the following two constituents add up to the reorganization energy (λ): firstly, a purely structural component (λ_i) should be considered, which include mainly vibrations of the

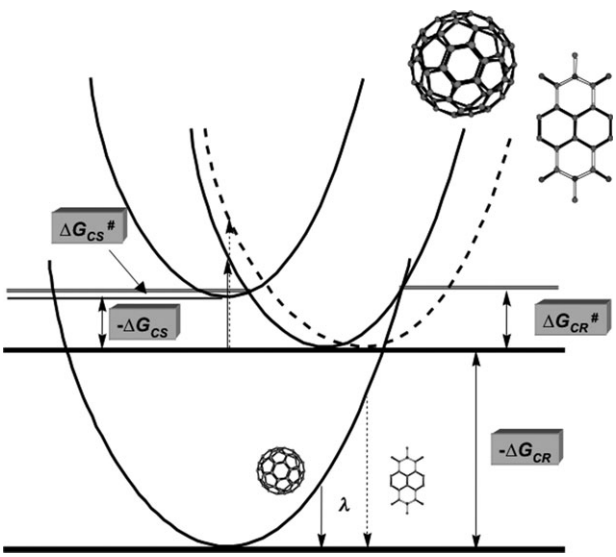

Fig. 1 Profile for the free energy surfaces for electron transfer in D–A_1 (A_1—solid line: spherical C_{60}) and D–A_2. (A_2—dashed line: planar naphthalenediimide).

molecules, *etc.*; secondly, contributions stemming from the polarization changes in the solvent environment (λ_S) play an important role. To this end, the characteristic λ emerges as one of the most significant parameters to understand interactions between solute and solvent before, during and after the electron transfer process.

Let's turn first to fullerenes, where several criteria are worth referring to. The high degree of delocalization within the extended π-system and its immediate impact on λ_i should be taken into account. A set of 60 molecular orbitals, which split into 30 bonding/30 antibonding π-molecular orbitals, evokes for C_{60} a five-fold degenerate HOMO (h_u) and a three-fold degenerate LUMO (t_{1u}).[12] They are separated by an energy gap of 1.8 eV. In line with three isoenergetic LUMO are electrochemical experiments that reveal six equally-spaced (*i.e.*, 450 ± 50 mV) reduction waves for C_{60}.[13] Such a unique separation is a clear manifestation for conditions that guarantee the optimal delocalization of charges, namely, electrons.

Calculating the bond reorganization energies (λ_B)—*via* an expedient bond-order-based method—adds more weight to the electrochemical measurements.[14] For C_{60}, $C_{60}^{\bullet -}$, C_{60}^{2-}, C_{60}^{3-}, C_{60}^{4-}, C_{60}^{5-} the bond reorganization energies are nearly identical. In other words, structural changes, such as bond length variations *etc.*, are similar upon adding electrons.

With regard to λ_i, the structural rigidity of the fullerene core is crucial. Particularly small Stokes-shifts were determined for C_{60} derivatives.[15] One may infer, for example, the fact that the force constants, controlling the vibrational levels in the first singlet excited state, resemble those in the singlet ground state. In fact, a low Franck–Condon instability energy of $\sim$20 cm^{-1} reflects the rigid structure found in fullerenes and their functionalized derivatives. Similar for each additional electron, the difference between the ground and one-electron reduced state, as expressed by Raman shifts of the totally symmetric "pentagonal pinch" mode, is negligible.[16] The exact experimental number is 6 cm^{-1} for C_{60}. In addition, for the insulating K_6C_{60} composition, reflecting the complete filling of the three-fold degenerate LUMO (t_{1u}), the vibrational frequency shifts from 1467 cm^{-1} to 1430 cm^{-1}, which corresponds to a frequency shift of 6 to 7 cm^{-1} per added electron.[17]

At last, the symmetrical shape and large size of fullerenes in general leads to small values for the solvent-dependent term (λ_S).[18] Implicit in λ_S is the energy that is associated with adjusting a newly generated state (*i.e.*, excited or reduced state) to a new solvent environment relative to its precursor state (*i.e.*, ground state). In other words, it is conceivable that solvent molecules in a solvation sphere are little perturbed by a small charge density. Notably, the charge density is highly delocalized in each carbon atom of fullerenes. This results in low values of λ_S even in highly polarizable solvents.

Most of the aforementioned rationales are also applicable for CNT. In fact, pioneering work by Weismann *et al.* on SWNT shed a detailed light onto the relationship between ground state absorption and excited state fluorescence.[19] Despite the large number of structural CNT present in their studies correlating emission, excitation and absorption spectra, a structural library was realized. Here, small Stokes-shifts of 65 cm^{-1} evolved.

When turning to Raman spectra of CNT, one particular mode is especially interesting: it is the so-called A_{1g} radial breathing mode.[20] Among three possible scenarios, namely, transversal radial (*i.e.*, orthogonal to the tube surface), longitudinal and transversal axial (*i.e.*, parallel to the tube surface) vibrations, the first one, which relates to the deformation orthogonal to the tubular axis, should be considered. The exact frequency of this mode scales inversely proportional with the nanotube diameter multiplied by a factor of 230 cm^{-1}.

To accommodate all these observations, we must conclude that in three- and one-dimensional nanometer scale carbon structures the electron acceptor in its ground, reduced and also excited state is similar. Therefore, changes in the equilibrium nuclear configurations, that is, the vertical displacement on the reaction coordinate, which are associated with the transformation of a molecule in a photoinduced charge-transfer reaction from an initial (*i.e.*, photoexcited state) to a final (*i.e.*, charge-separated state) are appreciably small.

First examples of charge-transfer systems—fullerenes

For intermolecular electron transfer processes of electron donors and electron acceptors at diffusional encounters, however, definitive evidence for the Marcus *inverted* region is almost nonexistent.[21] Notably, the rate constants for intermolecular reactions consist not only of an activation component (k_{act}), but also include a diffusion related term (k_{diff}), with the latter defining the upper limit of the observable rate. Thus, generally, the rate constant first increases with increasing the overall driving force as far as the following relationship holds: $k_{diff} > k_{act}$. Once k_{diff} starts to approach k_{act}, the rate constants enter the diffusional limit. Now, in most cases it remains at this purely diffusion-controlled level and only the Marcus *normal* and *top* region—assuming that k_{diff} is not too slow—is observed.

Several reasons might be considered to rationalize the failure in realizing the Marcus *inverted* region. Low k_{diff}, obscuring the decline of the overall rate, or the distribution of intermolecular donor acceptor distances on the energy gap are just two prominent examples. In the context of donor acceptor distances, enlargement of the driving force, especially into the highly exergonic region ($-\Delta_G^{\circ} \gg 0$), results in an increase in λ. Notably strong is the impact of λ_S to illustrate this, for a reaction between a particular donor and acceptor a larger solvent reorganization energy holds the rate constant large for greater energy gaps ($-\Delta G_{ET}^{\circ}$). A large λ_S means, however, a bigger encounter distance.

$$C_{60} + (\text{arene})^{\bullet +} \rightarrow (C_{60})^{\bullet +} + \text{arene} \qquad (1)$$

$$C_{76} + (\text{arene})^{\bullet +} \rightarrow (C_{76})^{\bullet +} + \text{arene} \qquad (2)$$

$$C_{78} + (\text{arene})^{\bullet +} \rightarrow (C_{78})^{\bullet +} + \text{arene} \qquad (3)$$

A breakthrough in this respect came from pulse radiolytic studies to test intermolecular charge shift reactions (k_{CSH}) from fullerenes (C_{60}, C_{76} and C_{78}) to a series of arene π-radical cations in dichloromethane (*i.e.*, eqn (1)–(3)).[22,23] Varying the oxidation strength of the arene π-radical cation, which was generated in a radical-induced oxidation evolving from the

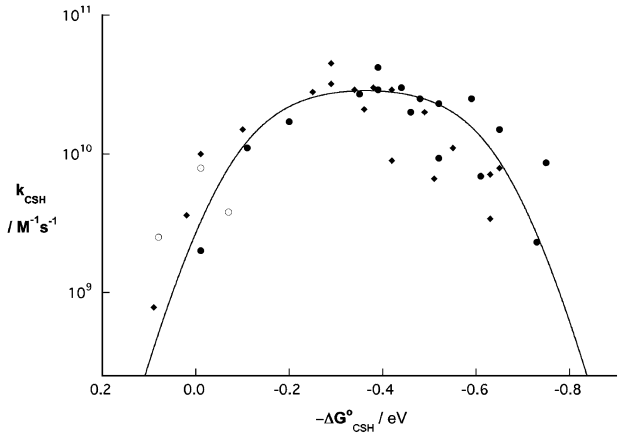

Fig. 2 Plot of log k_{CSH} *vs.* $-\Delta G_{CSH}$ for electron transfer from C_{60} (circle with interior point), C_{76} (solid circles) and C_{78} (hollow circles) to arene radical cations in dichloromethane. The solid line is drawn based on the Marcus theory of electron transfer.

solvent radical cation (dichloromethane)$^{\bullet+}$, helped to vary $-\Delta G^{\circ}_{CSH}$. In such charge-shift type electron transfer reactions, the solvation before and after the electron transfer may be largely cancelled out when the free energy change of the electron transfer is expected to be rather independent of the solvent polarity. On the other hand, the solvent reorganization energy for the electron transfer reaction is expected to decrease with decreasing the solvent polarity. Thus, this is an ideal system to examine whether fullerenes have a small intrinsic reorganization energy (λ) or not in a less polar solvent such as dichloromethane. Fig. 2 illustrates that the driving force dependence of k_{CSH} shows a pronounced decrease towards the highly exothermic region, representing the first definitive confirmation of the existence of the Marcus *inverted* region in a truly intermolecular electron transfer. The log k_{CSH} value increases with increasing the driving force to reach a diffusion-limited value, and then decreases with further increase in the driving force. Please note that k_{CSH} (2.3×10^{9} M^{-1} s^{-1}) for a highly exergonic electron transfer from C_{78} to the mesitylene radical cation ($-\Delta G^{\circ}_{CSH}$ = 0.73 eV) is about 20 times smaller than the value (4.5×10^{10} M^{-1} s^{-1}) for a much less exergonic electron transfer from C_{76} to, for example, the chrysene radical cation ($-\Delta G^{\circ}_{CSH}$ = 0.32 eV). From these experiments, an experimental value of *ca.* 0.36 ± 0.04 eV was deduced for the total reorganization energy of C_{76} and C_{78} in oxidative charge shift processes in dichloromethane.

Charge shift reactions—involving fullerenes—were alternatively studied *via* intermolecular electron transfer from a series of radiolytically generated metalloporphyrin π-radical anions, $(MP)^{\bullet-}$ (*i.e.*, eqn (4)).[23] This enabled the fine tuning of the reduction strength of the reducing species, with reduction potentials varying between −1.35 and −0.8 V *versus* SCE and, in turn, the variation of the free energy changes $-\Delta G^{\circ}_{CSH}$. Addition of various concentrations of C_{60} resulted in an accelerated decay of the absorption between 600 and 800 nm. The linear dependence of the observed rates on the C_{60} concentration supported the view that the $MP^{\bullet-}$ did indeed react with C_{60} *via* electron transfer. Most importantly, the grow-in rate of the $C_{60}^{\bullet-}$ absorption at various wavelengths in the 980–1100 nm range was nearly identical to the decay rate of the $MP^{\bullet-}$ absorption between 600 and 800 nm. Surprisingly, the rate constants for electron transfer between all the investigated $MP^{\bullet-}$ and C_{60} are found to be in the range of (1–3) × 10^{9} M^{-1} s^{-1}, despite the large variation in one-electron reduction potentials for the examined metalloporphyrins. The lack of dependence of the rate constant on the free energy change of the reaction has been ascribed to weak electronic interactions between the metalloporphyrins and C_{60} in the ground state. It should be noted, however, that no ground state charge-transfer interactions were detectable.

$$C_{60} + (MP)^{\bullet-} \rightarrow (C_{60})^{\bullet-} + MP \qquad (4)$$

Intermolecular electron transfer reactions were also studied with ZnP (*i.e.*, eqn (5)) and ZnPc (*i.e.*, eqns (6) and (7))—but in their triplet excited state.[24,25] Studies with ZnPc unravel an interesting twist.[25] Excitation of C_{60} in polar benzonitrile gives rise to the rapid formation of the C_{60} and ZnPc diagnostic π-radical anion and π-radical cation bands, respectively. In non-polar solvents—as a direct consequence of raising the energy levels for the charge separated radical pair—the electron transfer is shut off and, instead, the intriguing energy transfer route is activated.

$$^{3*}ZnP + C_{60} \rightarrow (ZnP)^{\bullet+} + (C_{60})^{\bullet-} \qquad (5)$$

$$^{3*}ZnPc + C_{60} \rightarrow (ZnPc)^{\bullet+} + (C_{60})^{\bullet-} \qquad (6)$$

$$ZnPc + {}^{3*}C_{60} \rightarrow (ZnPc)^{\bullet+} + (C_{60})^{\bullet-} \qquad (7a)$$

$$ZnPc + {}^{3*}C_{60} \rightarrow {}^{3*}ZnPc + C_{60} \qquad (7b)$$

Linearly shaped charge-transfer systems—fullerenes

As far as intramolecular electron transfer reactions are concerned, marked effects were seen in a study in which we probed a ZnP–C_{60} conjugate with van der Waals contacts—see Scheme 3.[26,27] The short separation (R_{ee}) of ~3.0 Å guaranteed that an intramolecular charge-separation succeeds in virtually any solvent and dominates over the competing energy transfer. The rapid formation and decay of $ZnP^{\bullet+}$ between 670–680 nm and $C_{60}^{\bullet-}$ around 900 nm in toluene testifies to the charge separation and charge recombination processes, respectively. Now, the systematic change in solvent polarity, for example, from non-polar toluene to polar benzonitrile,

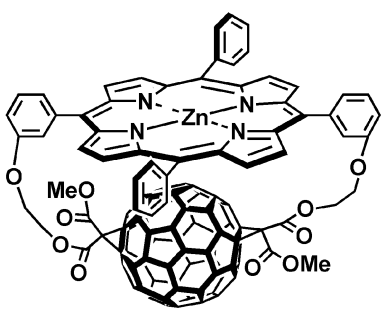

Scheme 3 π-stacked ZnP–C_{60} charge-transfer conjugate.

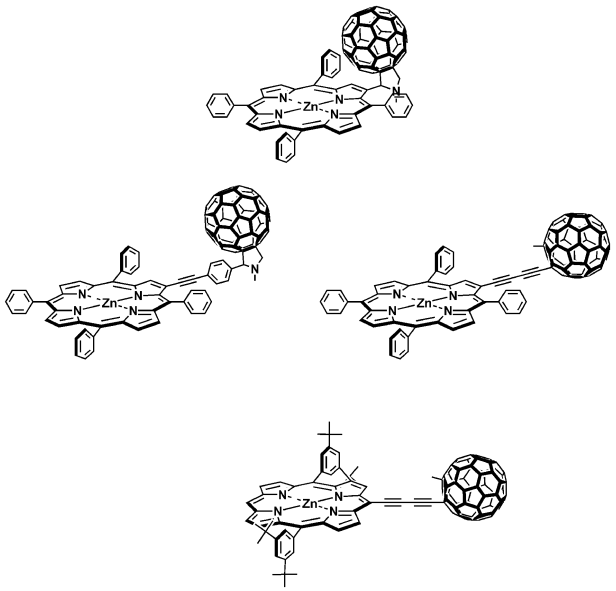

Scheme 4 Leading examples of short distance ZnP–C_{60} charge-transfer conjugates.

provided the powerful means to alter the free energy changes over a wide range—no change in the chemical structure deemed necessary. Indeed, a marked acceleration of the charge recombination rates was seen at smaller $-\Delta G^{\circ}_{CR}$, namely, at higher dielectric constants, which corroborated our working hypothesis. To illustrate this, the lifetimes varied over a wide range: 619 ps (toluene) to 38 ps (benzonitrile). Most importantly, correlating log k_{ET} with $-\Delta G^{\circ}_{ET}$ (*i.e.*, charge separation and charge recombination) and fitting of the resulting parabolic dependence yielded an experimental λ-value of 0.86 eV. The delocalization of electrons in C_{60}, provided by its large three-dimensional π-system, leads to the conclusion that the reorganization energy in the ZnP–C_{60} systems is not receptive towards large changes in the solvent polarity in going, for example, from toluene and THF to benzonitrile. Accordingly, the reorganization energies of the ZnP–C_{60} conjugate are reasonably assumed to be comparable in the different solvents.

Next, linear arrays were tested in which a systematic variation of R_{ee} separating the donor (ZnP) from the acceptor (C_{60}), to about 11.9 Å, leads to lifetimes of up to 2.7 μs in deoxygenated THF.[28] Notably, ZnP–C_{60} conjugates (Scheme 4), whose donor-acceptor distances fall essentially in between these limits—3.0 and 11.9 Å—reveal lifetimes that are typically on the order of several tens to hundreds of picoseconds.[29–31] In THF, values of 45 ps, 89 ps, 100 ps and 398 ps document some interesting trends: placing the same bridge at different positions of the porphyrin (*i.e.*, meso- *versus* pyrrole-position) and/or using different bridges (*i.e.*, ethynylene *versus* phenylene-ethynylene) impacts the electronic coupling element (V).

The reorganization energies describe a fundamental distance dependence: first they drop from 0.82 eV at R_{ee} = 3.0 Å to ~0.5 eV at R_{ee} = 6.18 Å and after that they steadily increase to 0.66 eV at R_{ee} = 11.9 Å. The electronic coupling, on the other hand, decreases monotonically with distance throughout the series, from 415 cm^{-1} at R_{ee} = 3.0 Å to 3.9 cm^{-1} at R_{ee} = 11.9 Å.

Similar effects were also seen for several H_2P–C_{60} conjugates.[28,29] An important consideration implies, however, that the higher oxidation potential of the $H_2P^{\bullet+}/H_2P$ couple relative to that of $ZnP^{\bullet+}$/ZnP of around 200 mV, would allow storing a larger fraction of the excited state energy as chemical potential in the charge-separated state. Slower k_{CS} and k_{CR} are logical consequences that stem from the energy gap variation in H_2P–C_{60} *versus* ZnP–C_{60} ensembles. For the pyrrole linked H_2P–C_{60} and ZnP–C_{60}, which are compared in Scheme 5,

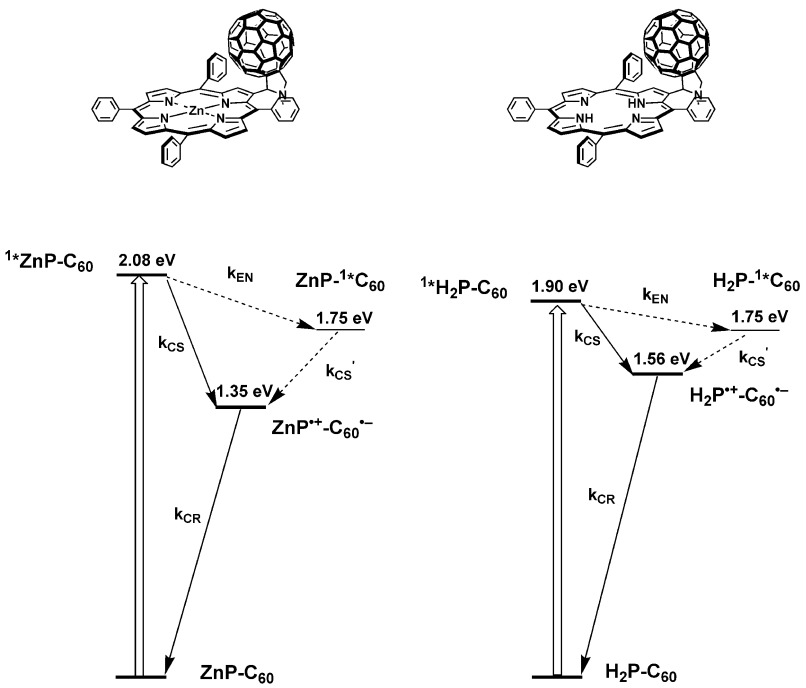

Scheme 5 Energetic and mechanistic comparison between ZnP–C_{60} and H_2P–C_{60} charge-transfer conjugates.

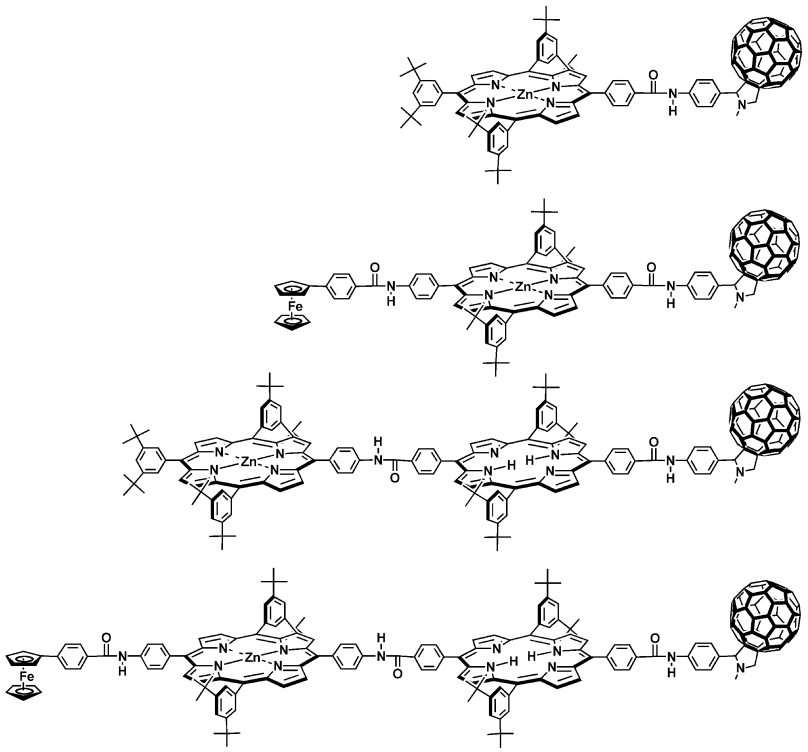

Scheme 6 Leading examples of long distance C_{60} charge-transfer conjugates: ZnP–C_{60}, Fc–ZnP–C_{60}, ZnP–H_2P–C_{60} and Fc–ZnP–H_2P–C_{60}.

radical ion pair state lifetimes of 290 ps and 50 ps, respectively, have been reported.

In an extension of that work, we reported on the first comprehensive assay of λ for intramolecular electron transfer involving C_{60} and planar naphthalenediimide (NIm).[32] In this context we probed a series of ZnP–C_{60} and ZnP–NIm conjugates endowed with similar rigid spacers. Importantly, in all ZnP–C_{60} the value of k_{CS} is much larger than the value of k_{CR}. Conversely, k_{CR} in the corresponding NIm-based dyad, ZnP–NIm, is much larger than k_{CS}, as determined by picosecond transient absorption spectrum and the decay of the ZnP fluorescence. λ and V are obtained from the intercept and the slope as 0.59 ± 0.15 eV and 7.9 ± 1.7 cm^{-1}, respectively. A linear correlation was also obtained for ZnP–Nlm, which afforded a much larger λ (1.41 ± 0.33 eV) together with a comparable V (7.8 ± 3.2 cm^{-1}). Such an extraordinary large difference in λ between the C_{60} and NIm conjugates is the reason why the k_{CS}/k_{CR} ratios are reversed in the two electron donor-acceptor conjugates and why the difference in charge recombination is as large as four orders of magnitude.

Encouraged by such remarkable results, several linear triads—with $R_{ee} \sim 30.3$ Å—and tetrads—with $R_{ee} \sim 48.9$ Å—were designed around the ZnP/C_{60} couple.[33] The first promising results stem from a set of molecular triads in which C_{60} is linked either to an array of two porphyrins (*i.e.*, ZnP–H_2P) or to a Fc–ZnP fragment—see Scheme 6. In ZnP–H_2P–C_{60}, the ZnP moiety performs as an antenna molecule, transferring its singlet excited state energy to H_2P. In polar benzonitrile, this energy transfer is followed by a sequential electron transfer yielding ZnP–$H_2P^{\bullet+}$–$C_{60}^{\bullet-}$ and subsequently $ZnP^{\bullet+}$–H_2P–$C_{60}^{\bullet-}$. Considering the overall efficiency of 40% for (i) funnelling light from the antenna chromophore (*i.e.*, ZnP) to the H_2P chromophore, (ii) charge injection into the fullerene core and (iii) charge shift, this artificial reaction center reproduces the natural system very well.

The lifetimes of $ZnP^{\bullet+}$–H_2P–$C_{60}^{\bullet-}$ correlate well with the solvent polarity: 34 μs (THF), 21 μs (benzonitrile), 20 μs (DMF). Since the driving force for charge recombination ($-\Delta G^{\circ}_{CR}$) decreases even in ZnP–H_2P–C_{60} with increasing solvent polarity, the observed trend suggests that the measured rate constants are in the Marcus *inverted* region.

The function of the Fc–ZnP–C_{60} and Fc–H_2P–C_{60} systems is limited to two consecutive electron transfers, yielding $Fc^{\bullet+}$–ZnP–$C_{60}^{\bullet-}$ and $Fc^{\bullet+}$–H_2P–$C_{60}^{\bullet-}$ in nearly 82 and 25%, respectively. In oxygen-free benzonitrile, $Fc^{\bullet+}$–ZnP–$C_{60}^{\bullet-}$ (1.3×10^5 s^{-1}) and $Fc^{\bullet+}$–H_2P–$C_{60}^{\bullet-}$ (1.2×10^5 s^{-1}) decay, however, considerably faster than what is seen for $ZnP^{\bullet+}$–H_2P–$C_{60}^{\bullet-}$ (4.8×10^4 s^{-1}). Taking into account the similarity in molecular structure and separation, $R_{ee} = 30.3$ Å, the different thermodynamics must be responsible for this intrinsic behavior. In fact, variation of $-\Delta G^{\circ}_{CR}$ (*i.e.*, comparing THF and DMF) indicated that the electron transfer kinetics within the $Fc^{\bullet+}/C_{60}^{\bullet-}$ couples are in the Marcus *normal* region.

Successful mimicry of the primary events in photosynthesis using ZnP–H_2P–C_{60} and Fc–ZnP–C_{60} encouraged us to combine these two systems into integrated single conjugates: Fc–ZnP–H_2P–C_{60} and Fc–ZnP–ZnP–C_{60}. The lifetimes of the spatially separated ($R_{ee} = 48.9$ Å) radical pairs, the products of a sequence of energy and multistep electron transfer reactions, reaches well beyond milliseconds (Fc–ZnP–H_2P–C_{60}: 0.38 s; Fc–ZnP–ZnP–C_{60}: 1.3 s), into a

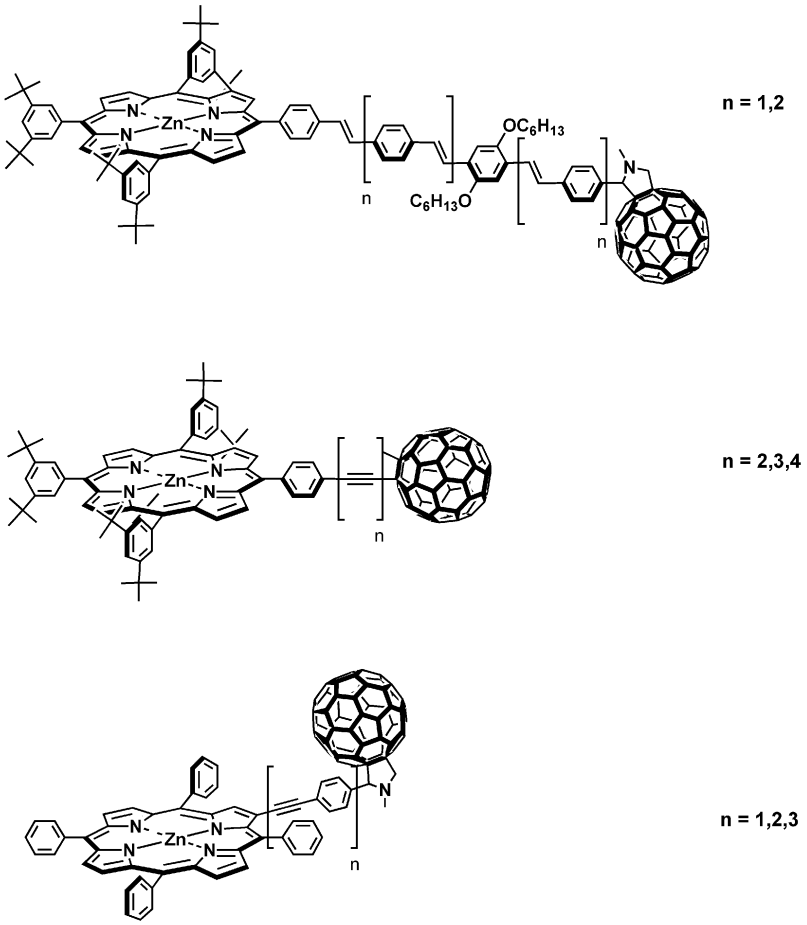

Scheme 7 Leading examples of molecular wire ZnP–C_{60} charge-transfer conjugates: oligo(*para*-phenylene vinylene), oligoalkyne and oligo(*para*-phenylene ethynylene).

time domain, which has never been accomplished so far in artificial photosynthetic reaction centers. The lifetime is comparable, for example, to the lifetimes of ~1 s in the bacteriochlorophyll dimer radical cation ($(Bchl)_2^{\bullet +}$)–secondary quinone radical anion ($Q_B^{\bullet -}$) ion pair in the purple bacterial photosynthetic reaction center.

The aforementioned cases demonstrate our success in controlling the radical ion pair state lifetime in C_{60}-containing electron donor–acceptor conjugates more or less at will. Placing donor and acceptor moieties in positions that they either assume van der Waals contacts or that they are separated by 5 nm impacts the lifetime values by nearly nine orders of magnitude. Key to this fundamental breakthrough is the choice of intervening spacers that mediate charges poorly. In fact, an electronic dumping factor (β) of 0.6 $Å^{-1}$ was determined when correlating the radical ion pair state lifetimes in ZnP–C_{60}, ZnP–H_2P–C_{60} and Fc–ZnP–H_2P–C_{60}.

Notably, integrating spacers that provide better conductance paths, as found in oligo(*para*-phenylene vinylene) (*i.e.*, $\beta = 0.02$ $Å^{-1}$)[34] or oligo(*para*-phenylene ethynylene) (*i.e.*, $\beta = 0.32$ $Å^{-1}$)[30,35], accelerates the charge transfer. Scheme 7 summarizes some leading examples. This holds likewise for k_{CS} and k_{CR}. At comparable donor–acceptor distances—$R_{ee} \sim 39$ Å—a lifetime of only 1.1 μs emerges, which is six orders of magnitude lower than those found in Fc–ZnP–H_2P–C_{60} or Fc–ZnP–ZnP–C_{60}. Somewhat larger are, however, the attenuation factors (*i.e.*, $\beta = 0.06 \pm 0.005$ $Å^{-1}$) found for oligoalkyne bridges.[31]

When comparing ZnP–C_{60} or H_2P–C_{60} conjugates with the related ZnPc–C_{60} or H_2Pc–C_{60} conjugates, a number of key differences should be highlighted.[36] Firstly, significant red-shifts of the visible absorption features are established (*i.e.*, ~600 nm *versus* ~700 nm). This favors unquestionably the utilization of light in the range of highest solar flux. Secondly, enhanced absorption cross-sections in the visible range of the solar spectrum (*i.e.*, $\varepsilon \sim 10\,000$ M^{-1} cm^{-1} *versus* $\varepsilon > 200\,000$ M^{-1} cm^{-1}) enhance the light harvesting in general. Thirdly, larger energy gaps (*i.e.*, $-\Delta G^{\circ}_{CS} < 0.7$ eV *versus* $-\Delta G^{\circ}_{CS} > 0.7$ eV) and faster rates evolve for the charge separation processes, which, in turn, assist in suppressing alternative deactivation channels for the singlet excited state, such as radiative and non-radiative decays. Finally, smaller energy gaps for the charge recombination step (*i.e.*, $-\Delta G^{\circ}_{CR}$) pulls these processes closer to the top of the Marcus parabola and, therefore, destabilizes the radical ion pair states. In this context, ZnP–C_{60} and ZnPc–C_{60}, which are compared in Scheme 8, give rise to radical ion pair lifetimes in THF of 50 ps and 49 ps, respectively.[35]

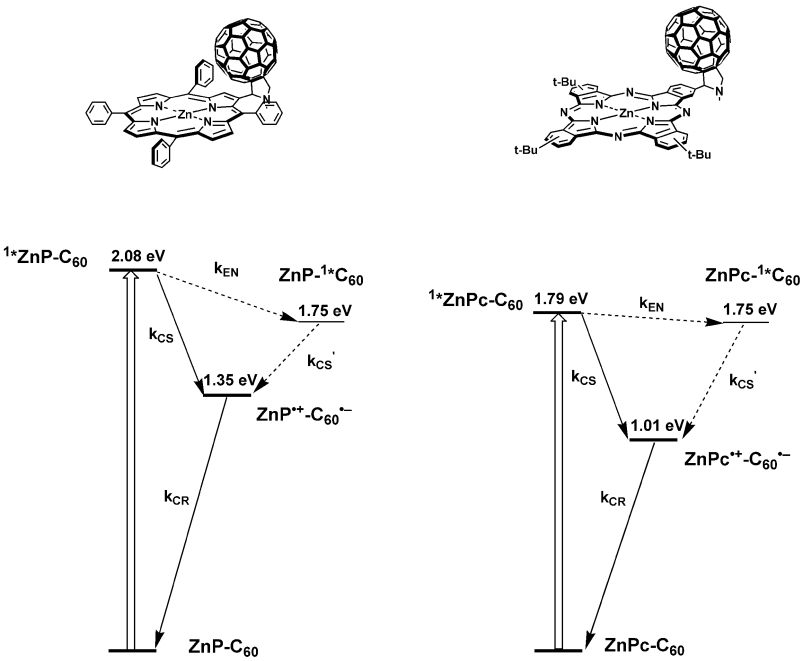

Scheme 8 Energetic and mechanistic comparison between ZnP–C_{60} and ZnPc–C_{60} charge-transfer conjugates.

Spherically-shaped charge-transfer ensembles: fullerenes

A first report on spherically-shaped ensembles documents the development of novel dendritic macromolecules, which form highly stable supramolecular hybrids with C_{60} in a well-defined fashion by virtue of strong interactions at the focal point of the cyclodimeric porphyrin cavity. Remarkably, the observed association constants (4.3×10^4 M^{-1}) are nearly two orders of magnitude larger than those with dendritic host molecules reported to date.[37]

Photochemical and photophysical properties of the triplet excited states of dendritic multiporphyrin arrays have been investigated by measuring the nanosecond transient absorption spectra in the visible and near-IR regions with changing the generation number, that is, first, third and seventh. In the presence of C_{60}, intermolecular charge separation takes place *via* the triplet excited states of the porphyrin. Deceleration of the electron transfer rate constants from the first to the third generation and the acceleration from the third to the seventh generation were observed, in which the latter tendency was interpreted by considering an increase in effective encounter radius. The observed small change of the rate constants for charge recombination between the oppositely charged species with the dendrimer generation was also reasonably interpreted by taking a smaller effective radius, due to electrostatic attraction, into consideration. Dendrimer generation effect was also observed for the intermolecular hole transfer process.[38]

The most recent example focuses on dendritic molecules appended with multiple ZnP—ranging from 6 to 24—that trap bipyridine compounds carrying multiple C_{60} (*i.e.*, one, two or three). Overall, coordination complexes are formed that bear photoactive layers consisting of spatially segregated donor and acceptor arrays on their surface. Upon increasing the number of these donor and acceptor units, the electron transfer reaction was remarkably facilitated, while the recombination of the resulting charge-separated state remained virtually intact. Within the new family, the largest k_{CS}/k_{CR} ratios (*i.e.*, 3400) are found when accommodating 24 ZnP units and roughly 30 C_{60} units on the dendrimer surface.[39]

One-dimensional charge-transfer systems: carbon nanotubes

An intriguing concept involves using the surface of semiconducting and metallic CNT as templates to integrate porphyrins or phthalocyanines that serve as visible light harvesting chromophores.

A first example reports on the efficient covalent tethering of SWNT with porphyrins through the esterification of SWNT-bound carboxylic acid groups—Scheme 9. Based on the initially established approach, the surface bound carboxylic acid groups were produced by acid treatment. In particular, the work started with two porphyrin derivatives containing terminal hydroxyl groups [5-(*p*-hydroxyhexyloxyphenyl)-10,15,20-tris(*p*-hexadecyloxyphenyl)-21H,23H-porphine] and [5-(*p*-hydroxymethylphenyl)-10,15,20-tris(*p*-hexadecyloxyphenyl)-21H,23H-porphine].[40] FTIR and thermal analysis indicated that amide or ester bonds were formed to bridge between the excited state electron donor and the SWNT. In the corresponding electron donor–acceptor nanoconjugates (*i.e.*, SWNT–H_2P), the photoexcited porphyrins deactivate through a transduction of excited state energy. Interestingly, the rates and efficiencies of the excited state transfer depend on the length of the tether that links the porphyrins with the SWNT. Thus, materials with shorter tethers showed the least fluorescence quenching.

Extending the scope of the aforementioned work, the carboxylic functionalities proved to be convenient for linking 5-*p*-hydroxyphenyl-10-15-20-tritolylporphyrin to either SWNT

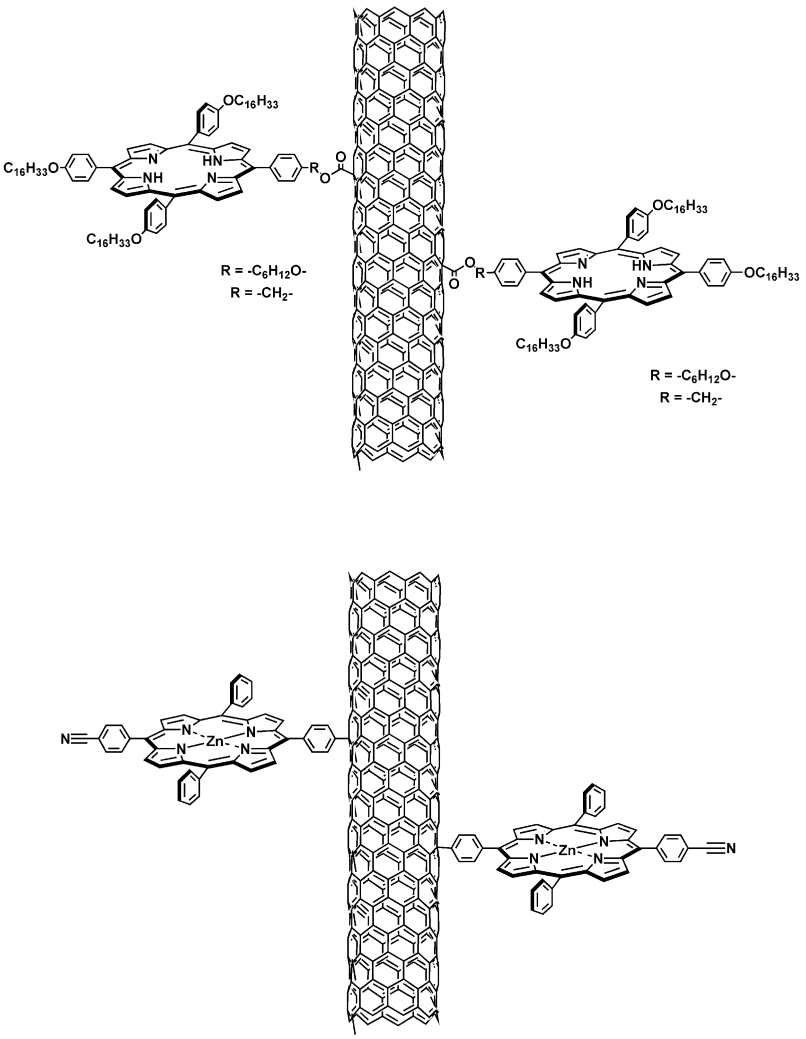

Scheme 9 Leading examples of SWNT charge-transfer nanoconjugates: SWNT–H_2P and SWNT–ZnP.

or MWNT.[41] According to thermogravimetric analyses, the amount of grafted porphyrins was estimated to range from 8 to 22%, depending on the initially-employed porphyrin concentrations.

Unsymmetrically-substituted aminophthalocyanines ZnPc were linked to SWNT through a reaction of the terminal carboxylic acid groups of shortened, chemically-etched SWNT.[42] However, the resulting materials are nearly insoluble in common organic solvents. The solubility/dispersability of the SWNT–ZnPc conjugates is, however, an indispensable task for a ready manipulation and a feasible solution phase processing.

Quite different is the approach represented in Scheme 10, which involves SWNT functionalization, namely, placing pyridyl isoxazolino functionalities along the sidewalls of short SWNT.[43] The synthesis is based on the 1,3-dipolar cycloaddition of a nitrile oxide onto SWNT. The resulting SWNT-py form complexes with ZnP. Formation of the SWNT-py/ZnP complex was firmly established by a detailed electrochemical study. However, photochemical excitation of the complex between SWNT-py/ZnP does not lead to electron transfer with the generation of charge-separated states. Fluorescence and laser flash studies indicate that the main process is energy transfer from the singlet excited state of ZnP to SWNT-py.

SWNT functionalization is also the basis when applying Suzuki coupling reactions (Scheme 9).[44] Recent work documents that this type of coupling reaction represents an efficient method for introducing ZnP onto the SWNT sidewalls. Despite all perceptions, covalently functionalized SWNT were

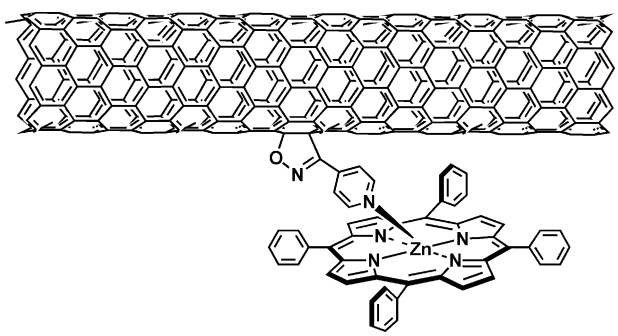

Scheme 10 SWNT-py/ZnP charge-transfer nanoconjugate.

found to serve as efficient quenchers even after their perfectly conjugated sidewall structure has been disrupted.

Still an important consideration when associating CNT with electron donor building blocks, is to preserve—as much as possible—the unique electronic structures of the CNT. A versatile approach involves grafting SWNT with polymers such as poly(sodium 4-styrenesulfonate) (SWNT–PSS^{n-}) with a SWNT-to-PSS^{n-} ratio of 55 : 45—see Scheme 11.[45] The attached PSS^{n-} functionalities also assist in exfoliating individual SWNT–PSS^{n-} from the larger bundles. AFM and TEM analysis corroborated the presence of SWNT with lengths reaching several micrometers and diameters around 1.2 nm. A Coulomb complex formation was achieved with SWNT–PSS^{n-} and an octapyridinium H_2P salt (H_2P^{8+}). Several spectroscopic techniques such as absorption, fluorescence, and TEM were used to monitor the complex formation between SWNT–PSS^{n-} and H_2P^{8+}, yielding SWNT–PSS^{n-}/H_2P^{8+}. Importantly, photoexcitation of H_2P^{8+} results in the newly-formed nanohybrid structure; an efficient intrahybrid charge separation event (0.3 ns). The charge separation is governed by a large thermodynamic driving force of 0.81 eV. The newly-formed radical ion pair exhibits a remarkably long lifetime of 14 μs under anaerobic conditions, which constitutes one of longest reported for any CNT ensemble found so far.

Similarly, dispersable SWNT—grafted with poly(4-vinylpyridine)—were tested in coordination assays with ZnP.[46] Grafting of the polymer to the sidewalls of SWNT was supported by Raman and near-IR spectra and the composition of the resulting SWNT–PVP was estimated as 61/39. AFM images and Raman spectra showed that the covalently-modified SWCNT-PVP (Scheme 11) exhibits either individual or thin bundles of SWNT. Kinetic and spectroscopic evidence corroborates the successful formation of SWNT–PVP/ZnP nanohybrids in solutions. Within this SWNT–PVP/ZnP nanohybrid, static electron transfer quenching 2.0 ($\pm$ 0.1) $\times$ 10^9 s^{-1} converts the photoexcited ZnP chromophore into a microsecond-lived radical ion pair state; that is, one-electron oxidized ZnP and reduced SWNT.

A series of SWNT that are functionalized with PAMAM dendrimers were recently described.[47] Importantly, the dendrimers are linked directly to the SWNT surface using a divergent methodology. This approach allows increasing the number of functional groups on the nanotubes without provoking significant damages to the conjugated π-system of SWNT. Scheme 12 shows that several tetraphenylporphyrin moieties can be linked to the periphery of the dendrimers. The photophysical properties of the resulting nanoconjugates (*i.e.*, SWNT–$(H_2P)_n$) have been investigated with a series of steady state and time resolved spectroscopy. The fluorescence kinetics provide evidence for two transient decays: one very short-lived (*i.e.*, 0.04 $\pm$ 0.01 ns) and one long-lived (*i.e.*, 8.6 $\pm$ 1.2 ns). A possible explanation is that some porphyrin units do not interact with the nanotubes, thus exhibiting a fluorescence lifetime similar to that of the free porphyrin. Complementary transient absorption measurements not only corroborate the fast decay of the photoexcited H_2P, but also confirm that intraconjugate charge separation evolves from the excited porphyrin to the SWNT.

Molecular organization: fullerenes

Organizing nanometer scale carbon structures with electron donor components that are dissimilar and sometimes incompatible brings about novel structural features, physical properties, and complex functions. These arise from the synergetic interactions of the individual constituents. The excitement about using biological organization principles stems from the ability to self-assemble and organize at near-atomic precision into structures with useful and predictable properties. In

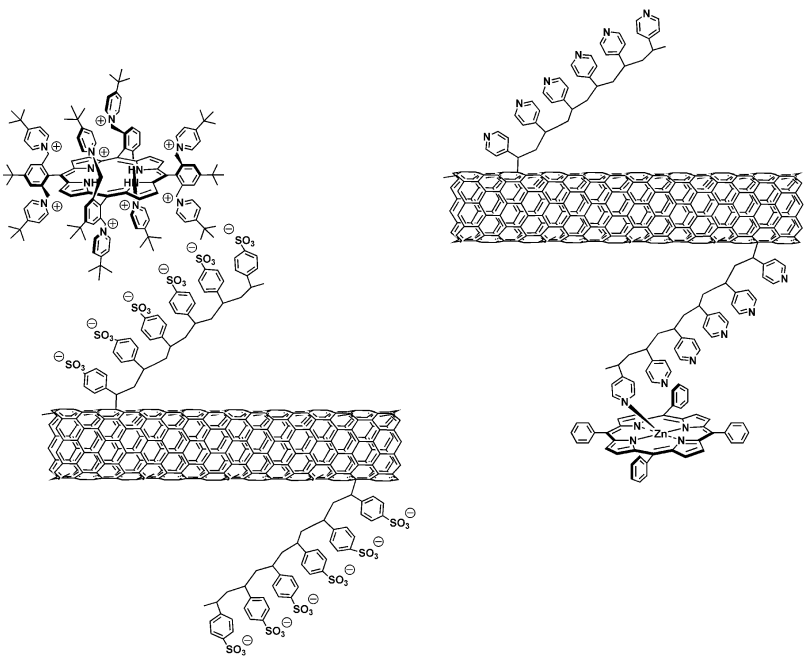

Scheme 11 Leading examples of SWNT charge-transfer nanoconjugates: SWNT–PSS^{n-}/H_2P^{8+} and SWNT–PVP/ZnP.

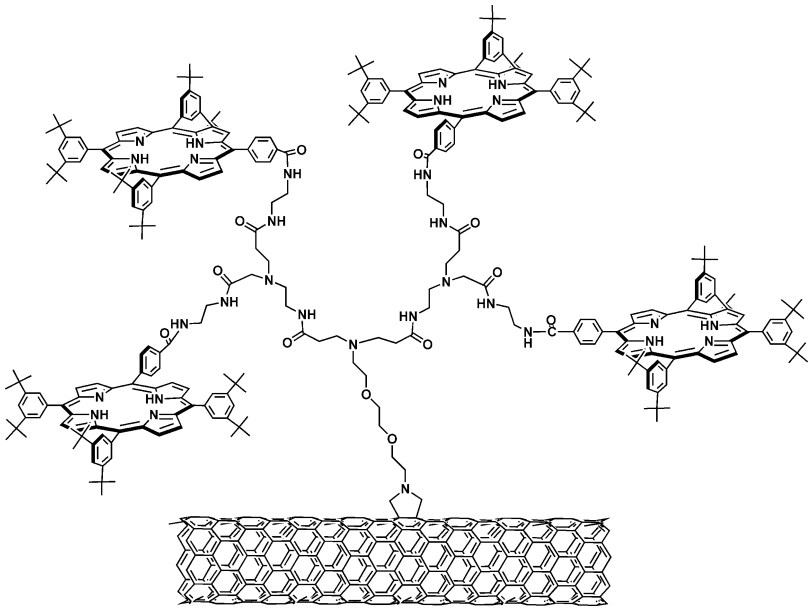

Scheme 12 Dendritic SWNT–$(H_2P)_n$ charge-transfer nanoconjugate.

addition, the ability of certain biological systems to handle enormous amounts of data and compute at high speeds should be considered. Biological methods are often more efficient, environmentally friendly, and overall superior to current technology.

C_{60} is a strongly hydrophobic and bulky compound. This all-carbon cage is virtually insoluble in polar media and has an equally strong and evident penchant towards solvents able to establish interactions with its π-electron system. Attaching polar/hydrophilic functionalities has also become a critical element to promote and modulate supramolecular aggregation; a process where factors such as growth, arrangement, and dimensions are being regulated. Solid samples of such functionalized fullerene can be directly introduced in aqueous media. The individual molecules extracted from amorphous solids diffuse into the liquid phase. Dipolar interactions between the ionic moiety and water molecules are responsible for the solvation process, which is usually further increased by ultrasonic treatment. In contrast, the lack of dipolar interactions completely prevents dissolution of pristine fullerenes.

Solvent variations promote the self assembly—into either nanorods or vesicles—of fullerenes functionalized with an ionic group.[48] This notion was confirmed through the investigation of the supramolecular behavior in aqueous media of three C_{60} derivatives (Fig. 3). When the fullerene core carries a short organic side-chain, which is terminated by an ionic ammonium group—after solubilization assisted by ultrasonication—exclusively spherical nanostructures with an average diameter of 800 nm are noted (Fig. 3a).

Next, we look at fullerene derivatives that carry a long side-chain (Fig. 3b and c). In one of them, a second charge is located on the nitrogen atom of the pyrrolidine ring, which was introduced to enhance its hydrophilicity and therefore its solubility in water. Differently from the aforementioned case, these two systems form rod-like supramolecular nanostructures. The nanorods are several microns long, have a diameter of about 4 nm and form uniform bundles. These observations corroborate the hypothesis that the size of the functional group attached to C_{60} determines the shape of the final aggregate.

All the molecules discussed above have two elements of ordering, the hydrophobic fullerene cage and the hydrophilic ionic group. In the following, a third element of ordering was added. It is known that porphyrin and/or phthalocyanine groups favor π-stacking interactions among themselves and with fullerenes. Sonication-assisted solubilization of C_{60}–H_2P salt (Scheme 13) in water led to a completely different nanostructure. The one-dimensional nanotubules have uniform dimensions typically reaching 30 nm in diameter and 500 nm in length. In this case, the strong interactions that favor the formation of nanoaggregates are either porphyrin–porphyrin or C_{60}–porphyrin and are several times larger than the C_{60}–C_{60} interactions.

Induction of self organization between ZnPc and C_{60} moieties in an amphiphilic ZnPc–C_{60} salt, which occurs predominantly through intermolecular forces, results in uniformly nanostructured one-dimensional nanotubules.[49] Their photoreactivity, in terms of an ultrafast (*i.e.*, $\sim 10^{12}$ s^{-1}) charge separation and ultraslow charge recombination (*i.e.*, $\sim 10^3$ s^{-1}), is remarkable. In addition, the observed $ZnPc^{\bullet+}$–$C_{60}^{\bullet-}$ lifetime of 1.4 ms implies, relative to the monomeric ZnPc–C_{60}, an impressive stabilization of six orders of magnitude. Clearly, the charge separation lifetime found in ZnPc–C_{60} one-dimensional nanotubules reaches into a time domain typically found in thin solid films of donor acceptor composites.

Control over molecular organization is also accomplished when spreading solutions of amphiphilic fullerene derivatives at the air-water interface.[50,51] In fact, a single monolayer, tightly packed coverage was only found when the balance between hydrophilicity and hydrophobicity is appropriate. Notably, the balance between hydrophobic and hydrophilic

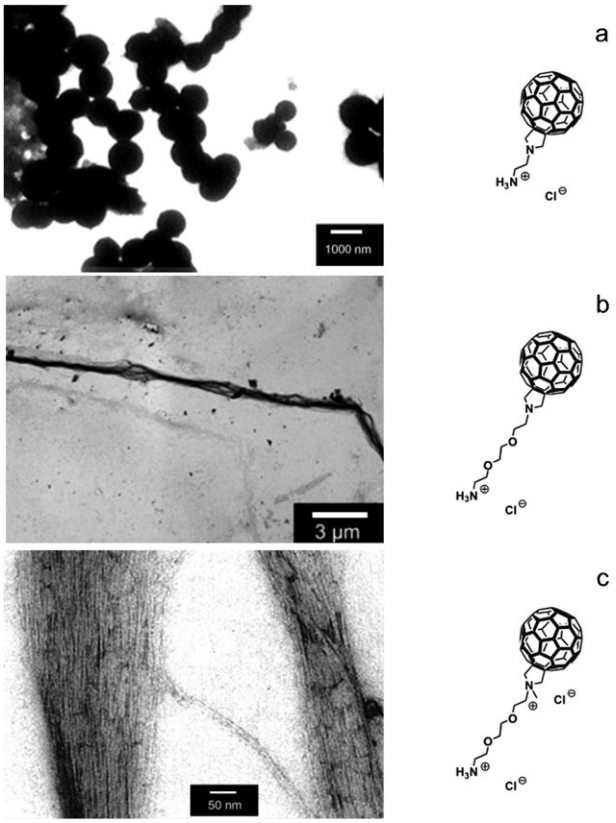

Fig. 3 Ordering fullerene materials at nanometer dimensions.

interactions is so delicate that it was possible to trigger and observe phase transitions (*i.e.*, structural rearrangements) in the monolayers. At first glance, the products of the cooperative rearrangements are uniformly oriented rods. They are

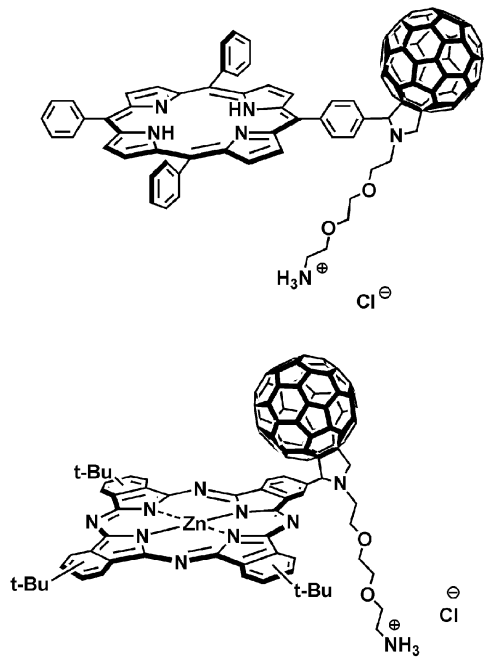

Scheme 13 Leading examples of amphiphilic C_{60} charge-transfer conjugates: H_2P–C_{60} and ZnPc–C_{60} salts.

several hundred micrometers long and have an outside diameter of $\sim 1.1 \pm 0.2$ μm. A closer look reveals that the inner structure depend on the hydrophilic functionality. For instance, the all equatorial *e,e,e*-$C_{60}[C(COOH)_2]_3$ leads to rods that are formed from well-ordered layers where the fullerenes arrange into a hexagonal pattern. Of equal importance are side groups, which govern the supramolecular organization. The presence of six polar termini in *e,e,e*-$C_{60}[C(COOH)_2]_3$, in the all-equatorial arrangement, promotes the formation of hexagonal patterns.

An alternative to force structural ordering in solution or at the air–water interface (*vide infra*) is the use of polyelectrolyte surfaces. Here, an important requisite is the presence of ionic functionalities in the molecule. Pyrrolidinium ions, which add amphiphilic character to C_{60}, are probate means.[52] Orderly assemblies were found in cases that are either flexible (*i.e.*, oligoethylene glycol bridges) or rigid (*i.e.*, androstane bridge), but strong differences emerge. For the flexible system, topographic images of the surfaces show fine-grained structures—with two-dimensional aggregates of 20–50 nm sizes—that develop into a continuous uniform film. A surprisingly high level of intermolecular organization characterized by linear aggregates, typically 10 nm in height and 1–3 μm in length, emerge for the rigid system. The organization is the outcome of the structural anisotropy, which is larger for the rigid compound. Importantly, water inhibits the formation of the rods, and films with regular grain morphology (*i.e.*, 20–50 nm-sized nanoaggregates) are obtained. When only 10 vol% of water is added to the DMSO solution, an intermediate morphology appeared characterized by a two-dimensional network of spaghetti.

Molecular organization: carbon nanotubes

While supramolecular interactions play only a secondary role when dealing with fullerenes, they have been implemented as a major player in the field of CNT, especially in the context of dispersing CNT.

As a leading example our recent success in the facile supramolecular association of pristine SWNT with linearly-polymerized porphyrin polymers towards versatile electron donor–acceptor nanohybrids should be considered.[53] The target SWNT nanohybrids, which are dispersable in organic media, were realized through the use of soluble and redox-inert poly(methylmethacrylate) (PMMA) bearing surface immobilized porphyrins (*i.e.*, H_2P–polymer). Conclusive evidence for H_2P–polymer/SWNT interactions came from absorption spectroscopy: the fingerprints of SWNT and H_2P-polymer are discernable throughout the UV, VIS, and NIR part of the spectrum. A similar conclusion was also derived from TEM and AFM. AFM images illustrate, for example, the debundling of individual SWNT. An additional feature of H_2P–polymer/SWNT is an intrahybrid charge separation, which has been shown to last for 2.1 ± 0.1 μs.

Following an essentially similar strategy, SWNT were found to strongly interact with a highly soluble, conjugated ZnP–polymer,[54] a novel triply fused ZnP–trimer,[55] and just ZnP[56] (Scheme 14)—a rare earth phthalocyanine (*i.e.*, $HErPc_2$)[57] and a tetraformylporphyrin/diaminopyrene

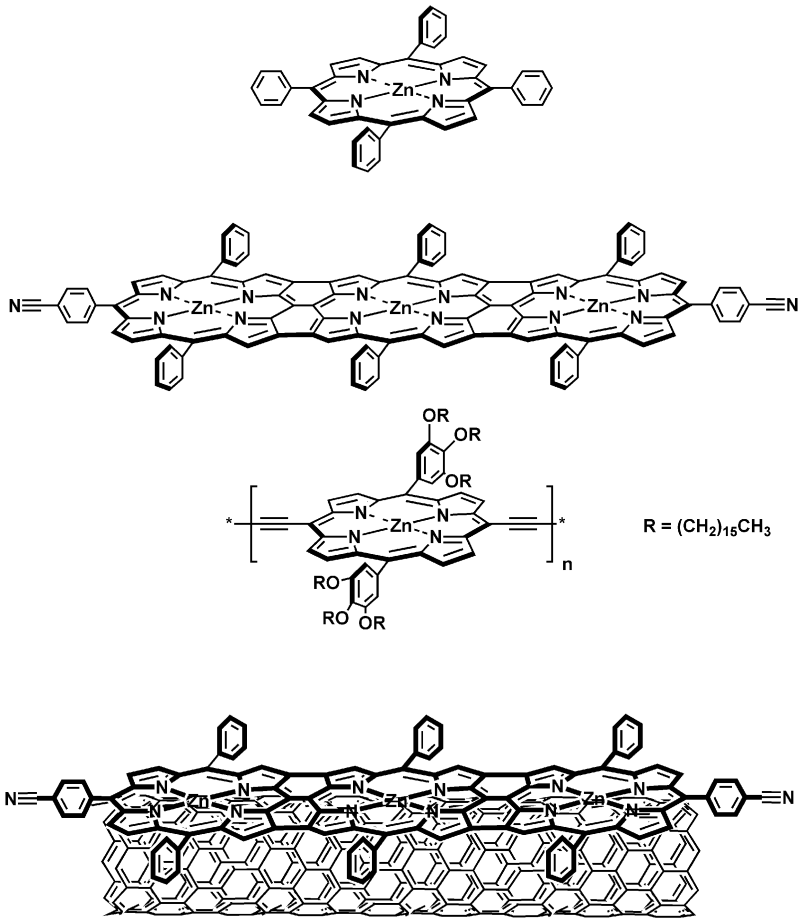

Scheme 14 Leading examples of SWNT charge-transfer nanohybrids: SWNT/ZnP, SWNT/ZnP-trimer and SWNT/ZnP-polymer.

polymer[58] were also tested. Successful complexation with, for example, the ZnP–polymer was manifested in a 127 nm bathochromic shift of the Q-band absorption. Additional evidence for interactions between the ZnP–polymer, ZnP–trimer and ZnP and SWNT was obtained from fluorescence spectra, where the ZnP fluorescence was significantly quenched. The fluorescence quenching has been ascribed to energy transfer between the photoexcited porphyrin and SWNT.

Generally, SWNT interactions with H_2P turned out to be appreciably stronger than what is typically seen when employing ZnP.[56] AFM images of, for example, SWNT/H_2P revealed smaller bundle sizes than those recorded for SWNT/ZnP with even some individual specimen (*i.e.*, diameters of 1.5 ± 0.2 nm). Overall, SWNT/H_2P interactions open the way to suspensions that are more stable than those of SWNT/ZnP.

The trend of stability was further corroborated with a water-soluble H_2P derivative, namely, [meso-(tetrakis-4-sulfonatophenyl) porphine dihydrochloride].[59] In these SWNT suspensions, which were shown to be stable for several weeks, eminent interactions protect H_2P against protonations to the corresponding diacid. Moreover, these strongly interacting hybrids have been successfully aligned onto hydrophilic polydimethylsiloxane surfaces by flowing SWNT solutions along a desired direction and then transferred to silicon substrates by stamping.

Of interest is the following work: SWNT were effectively worked-up with H_2P–[5,10,15,20-tetrakis(hexadecyloxyphenyl)-21*H*,23*H*-porphine].[60] The insoluble and recovered SWNT were separated from H_2P by treatment with acetic acid and vigorous centrifugation. After heating the recovered SWNT and the free SWNT to 800 °C in a nitrogen atmosphere, the spectroscopic analysis showed that the semiconducting SWNT and the free SWNT are enriched in recovered and metallic SWNT, respectively. We must assume selective interactions between H_2P and semiconducting SWNT as the inception to a successful separation of metallic and semiconducting nanotubes.

Ionic pyrene derivatives (*i.e.*, 1-(trimethylammonium acetyl) pyrene (pyrene$^+$)—Scheme 15) were used to solubilize SWNT through π–π interactions with solubilities as high as 0.2 mg ml^{-1} and a stability that reaches several months under ambient conditions without showing any apparent precipitations.[61] In terms of electronic interactions between the two π-systems, the most important data stem from steady-state voltammetry with SWNT/pyrene$^+$: large potential shifts of 0.4 V with respect to free pyrene$^+$. Now that the surface of SCNT is covered with positively-charged ionic head groups, van der Waals and electrostatic interactions are utilized to complex oppositely-charged electron donors. Water-soluble porphyrins 5,15-bis-[2′,6′-bis-2″,2″-bis-(carboxy)-ethyl-methyl-4′-*tert*-butyl-pheny]-10,20-bis-(4′-*tert*-butylphenyl) porphyrin octasodium (H_2P^{8-}) salt and the related

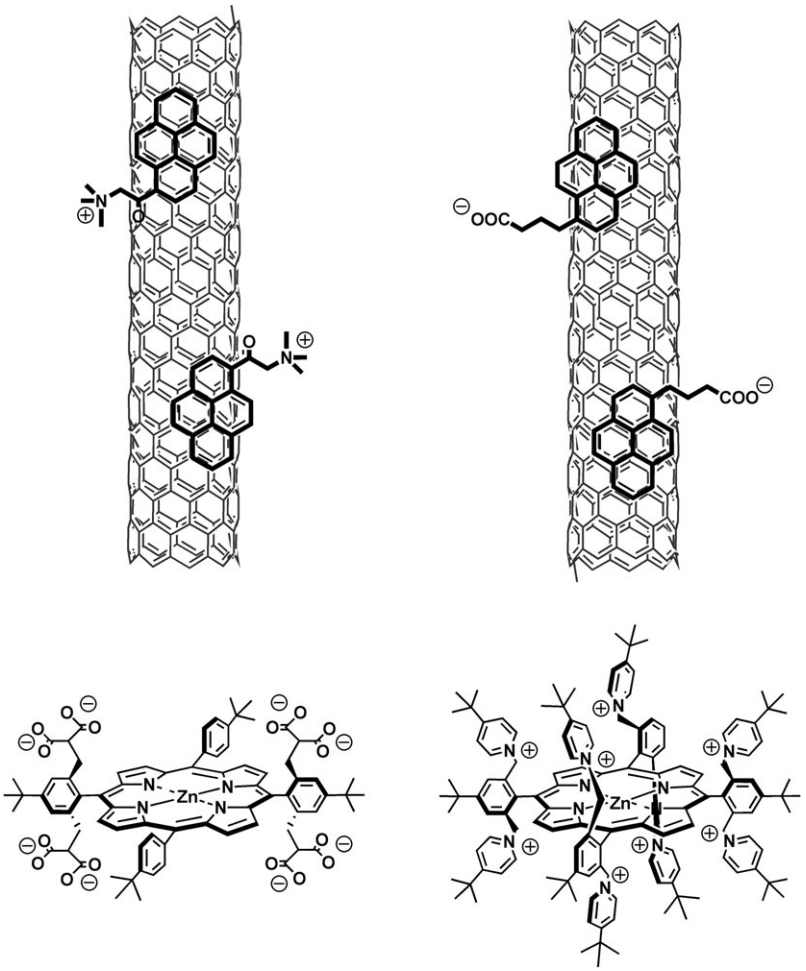

Scheme 15 Leading examples of SWNT charge-transfer nanohybrids: SWNT/pyrene^{+}/ZnP^{8-} and SWNT/pyrene^{-}/ZnP^{8+}.

zinc complex (ZnP^{8-}) were selected as ideal candidates for the development of SWNT-based photo-active systems. In the composite systems, fluorescence and transition absorption studies showed rapid intrahybrid electron transfer (0.2 ± 0.05 ns). The driving force for photoinduced electron transfer reactions is appreciably large with values around 1.0 eV. The differential absorption changes of the SWNT/pyrene^{+}/ZnP^{8-} or SWNT/pyrene^{+}/H$_2$P^{8-} assemblies are governed by broad absorptions in the visible spectrum between 600–800 nm because of ZnP^{8-}- or H$_2$P^{8-}-centered redox products.

Multiple concentric cylindrical graphitic tubes MWNT are more suitable for achieving charge transfer and charge transport. MWNT interact similarly to SWNT with pyrene^{+} and produce stable nanocomposites.[62] Interestingly, a better delocalization of electrons in MWNT helps to significantly enhance the stability of the radical ion pair (5.8 ± 0.2 microseconds) relative to the analogous SWNT (0.4 ± 0.05 microseconds). Percolation of the charge inside the concentric wires in MWNT decelerates the decay dynamics that are associated with the charge recombination.

Applying similar π–π interactions, SWNT were integrated with a series of negatively-charged pyrene derivatives (pyrene^{-}), such as 1-pyreneacetic acid, 1-pyrenecarboxylic acid, 1-pyrenebutyric acid, 8-hydroxy-1,3,6-pyrenetrisulfonic acid and a series of water soluble, positively-charged porphyrins into functional nanohybrids through a combination of associative van der Waals and electrostatic interactions.[63] Solubilities of SWNT/pyrene^{-} nanocomposites were around 2.0 mg mL^{-1}. The resulting nanohybrids were photoexcited with visible light, and found to behave similar to the previously described systems.

Thin-film photovoltaics and photoelectrochemical cells. The requirement to develop inexpensive renewable energy sources has stimulated new approaches for the production of efficient, low cost organic photovoltaic devices.[1] Particular attention has been drawn in recent years towards developing bulk heterojunction organic solar cells, which possess an active layer of a conjugated polymer as electron donor. Here, nanometer scale carbon structures—C_{60} and CNT—usually serve as electron acceptors.[64] The quest is to integrate carbon nanostructures together with porphyrins or phthalocyanines into multifunctional hybrid cells that reveal considerable promise for applications as photochemical energy conversion systems. Please note that sometimes very different photocurrent characterization conditions (*i.e.*, light power, intensities, size of the cells, *etc.*) were used, which limits a meaningful comparison.

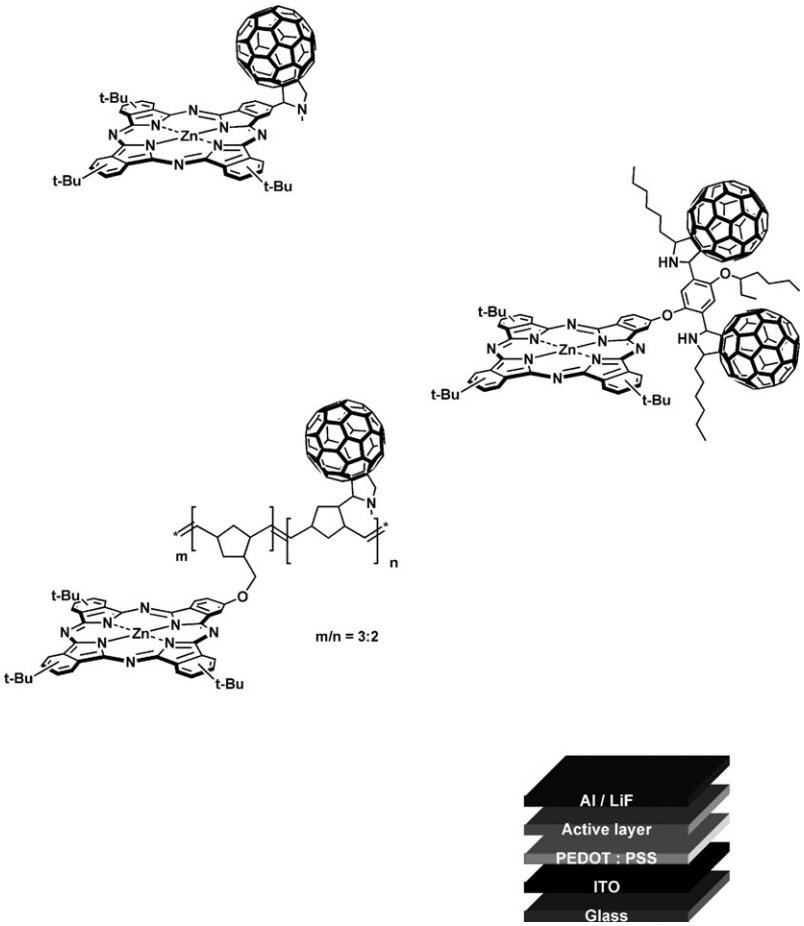

Scheme 16 Leading examples of ZnPc–C_{60} charge-transfer conjugates for photovoltaic cells: ZnPc–C_{60}, ZnPc–$(C_{60})_2$ and ZnPc/C_{60} polymer.

Thin-film photovoltaics

Thin-film photovoltaics made from bulk heterojunctions are made by drop casting or spin-coating. The morphology of the active layer in these devices has garnered particular interest because electron transfer from the donating polymer to the accepting fullerene occurs over a distance of *ca.* 10 nm, suggesting that an interpenetrating network of that length scale is necessary for maximum device performance.[65]

A first demonstration of a working solar cell—Scheme 16—using ZnPc–C_{60} as the active material led to power conversion efficiencies under simulated solar illumination of 0.02%.[66] This is a promising result for application of ZnPc–C_{60} to photovoltaics. Increasing the C_{60} content—similar to in C_{60}/polymer blends—prompted us to create and test a ZnPc–$(C_{60})_2$.[67] Here, notable charge transport problems were, however, hampering meaningful improvements of the device performance.

An improvement was noted in a ZnPc/C_{60} polymer material that is based on a polynorbornene framework to which the photo- and electroactive ZnPc and C_{60} are randomly attached as pendant units.[68] This material has been prepared by ring-opening metathesis polymerisation. Moderate power conversion efficiencies of $\sim$0.04% demonstrate this trend.

Photoelectrochemical cells

Self assembled monolayers of ZnP/C_{60} and H_2P/C_{60} conjugates (*i.e.*, covalent), is by far the most frequently and systematically studied approach for the construction of nanostructured photoelectrodes.[69] In particular, covalently linked dyad and triad conjugates involving porphyrins and C_{60} with a thiol functionality have been self assembled onto gold electrodes for photocurrent measurements. Cathodic photocurrents were observed upon irradiation of the modified gold electrodes, in which ZnP-containing cells revealed better performance than the analogous H_2P cells. Further performance improvements were noted when boron dipyrrin was coassembled as an antenna—improving the absorption in the green and in the blue region.[70] However, strong excited state quenching of the porphyrin by the gold surface is the limiting factor that prevents attaining higher charge separation quantum yields.

Highly transparent (>90%) and conductive indium tin oxide (ITO) support electrodes are much better suited for nanostructured photoelectrodes than the aforementioned gold electrodes, due to the lack of porphyrin singlet excited state quenching.[71] Thiol or siloxy groups were chosen as chemical linkers that help to bind, for example, H_2P–C_{60} conjugates (Scheme 17) to the electrode surface. In the case of siloxy

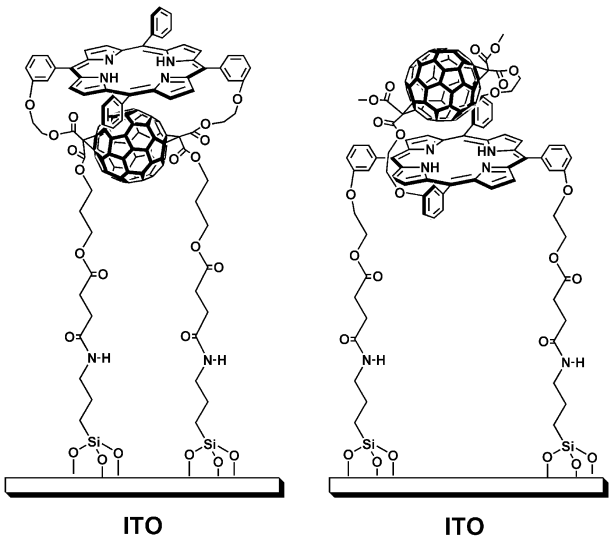

Scheme 17 Leading examples of H_2P–C_{60} charge-transfer conjugates for photoelectrochemical cells.

groups, the conjugates contain two linkers for connecting the H_2P and C_{60} moieties and enforcing them essentially to similar geometries of the donor–acceptor couple, and two linkers to ensure the attachment of the dyads to the ITO surface with two desired opposite orientations.[72] Placing C_{60} between ITO and H_2P shows photocurrents that are 25 times higher than that for the reversed ordering. Among the fullerene–porphyrin conjugates that bear multiporphyrin arrays/dendrimers H_2P instead of ZnP led to higher photocurrent conversion efficiencies.

More recently, a self assembled monolayer of a ZnP–C_{60} conjugate, in which a triosmium carbonyl cluster moiety links C_{60} and a porphyrin unit and 3-(triethoxysilyl)propyl isocyanide as a surface anchoring ligand, is shown to exhibit the highest photocurrent efficiency ever reported for a covalently linked systems.[73]

The hybrid strategy (*i.e.*, non-covalent) is in general more promising/effective because the photocurrent conversion efficiency has often been limited by the poor vectorial electron flow in covalently linked conjugates.[74] For example, non-covalent fullerene–porphyrin hybrids that rely on hydrogen bonding, van der Waals, π–π, and electrostatic interactions have been shown to be suited for the construction of nanostructured photoelectrodes. Most efficient photocurrent generations were accomplished when well tailored energy and redox gradients, in hybrid structures of fullerenes, porphyrins and ferrocenes were constructed.

An alternative concept to organic solar cells relies on the quaternary self organization of H_2P and C_{60} *via* their clusterization with gold nanoparticles on nanostructured SnO_2 electrodes.[75] First, porphyrin–alkanethiolate monolayer-protected gold nanoparticles are prepared (*i.e.*, secondary organization) starting from the primary porphyrin–alkanethiol component. In this context, the effective π–π interactions between H_2P and C_{60} in solutions and in the solid state are important as a means towards donor–acceptor nanoclusters that are characterized by an interpenetrating network and an enhanced light harvesting throughout the solar spectrum. In fact, the porphyrin-modified gold nanoparticles were found to form complexes with C_{60} (*i.e.*, tertiary organization), and they are clustered in a solvent mixture of acetonitrile and toluene (*i.e.*, quaternary organization). The highly colored composite clusters can then be assembled as three-dimensional arrays onto nanostructured SnO_2 films to afford photoelectrodes using an electrophoretic deposition method. The corresponding films exhibit incident photon-to-photocurrent efficiencies as high as 54% and broad photocurrent action spectra. The power conversion efficiency of the composite electrode reaches as high as 1.5%, which is 45 times higher than that of the reference system, namely, the individual porphyrin and fullerene components.

A remarkably high power conversion efficiency of nearly 1.3% and a maximum incident photon-to-photocurrent efficiency of 42% were attained using composite clusters of

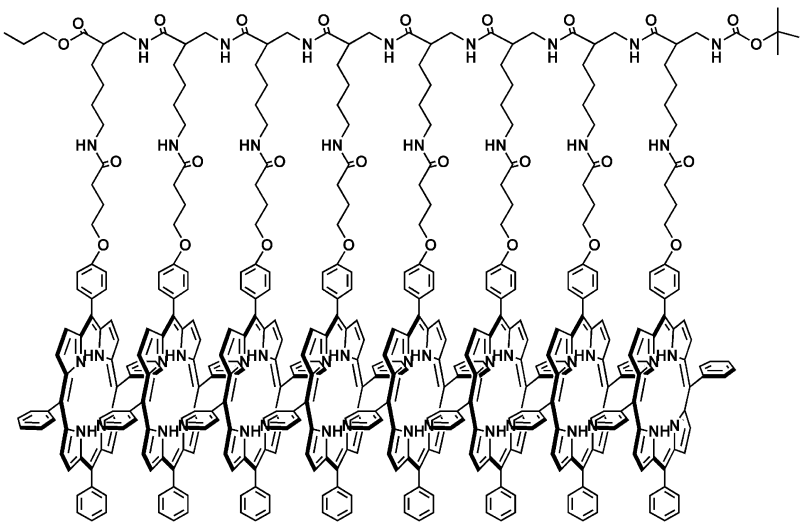

Scheme 18 H_2P–peptide octamer for photoelectrochemical cells.

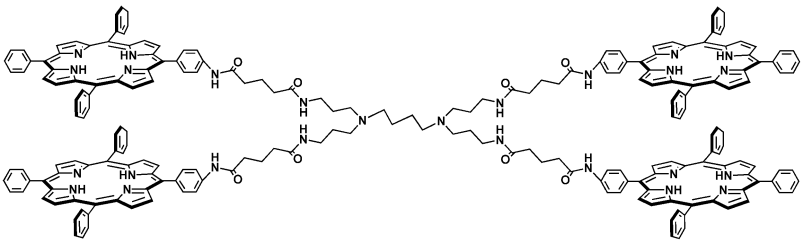

Scheme 19 H_2P–dendrimer for photoelectrochemical cells.

H_2P–peptide octamer and C_{60}—without, however, the use of gold nanoparticles—see Schemes 18 and 19.[76] Using a H_2P-dendrimer as electron donor, the photon-to-photocurrent efficiency drops—under comparable conditions—to 15%. A reference, H_2P–C_{60}, shows only 0.4%.[77]

Some initial promising reports on photoelectrochemical devices integrating SWNT—as electron acceptor—on ITO are based on non-covalent assembly strategies. In most of these instances, the ITO electrodes were covered with a base layer of polyelectrolyte (*i.e.*, poly(diallyl-dimethylammonium)chloride ($PDDA^{n+}$) or sodium polystyrene-4-sulfonate (PSS^{n-})) through hydrophobic–hydrophobic forces—Scheme 20.[78,79] A proper grafting of SWNT with pyrene derivatives bearing polar functional groups permits one to disperse them in aqueous media and to assemble them electrostatically on the polyelectrolyte base layer. In the final step, water soluble but oppositely-charged porphyrins were assembled as the top layer. This approach has been extended to double wall carbon nanotubes (DWNT), MWNT and thin-MWNT. Importantly, thin-MWNT showed the best performance as electron acceptor layer material with monochromatic power-conversion efficiencies of up to 10.7% for a device that contains a single layer of thin-MWNT and a single layer of ZnP.

Photoelectrochemical solar cells were also designed with a light harvesting nanoarchitecture consisting of SWNT and porphyrin moieties.[80] In this particular work, molecular assemblies of protonated porphyrin and SWNT were assembled as three-dimensional arrays onto nanostructured SnO_2 films by an electrophoretic deposition method. The composite cluster electrode exhibits an incident photon-

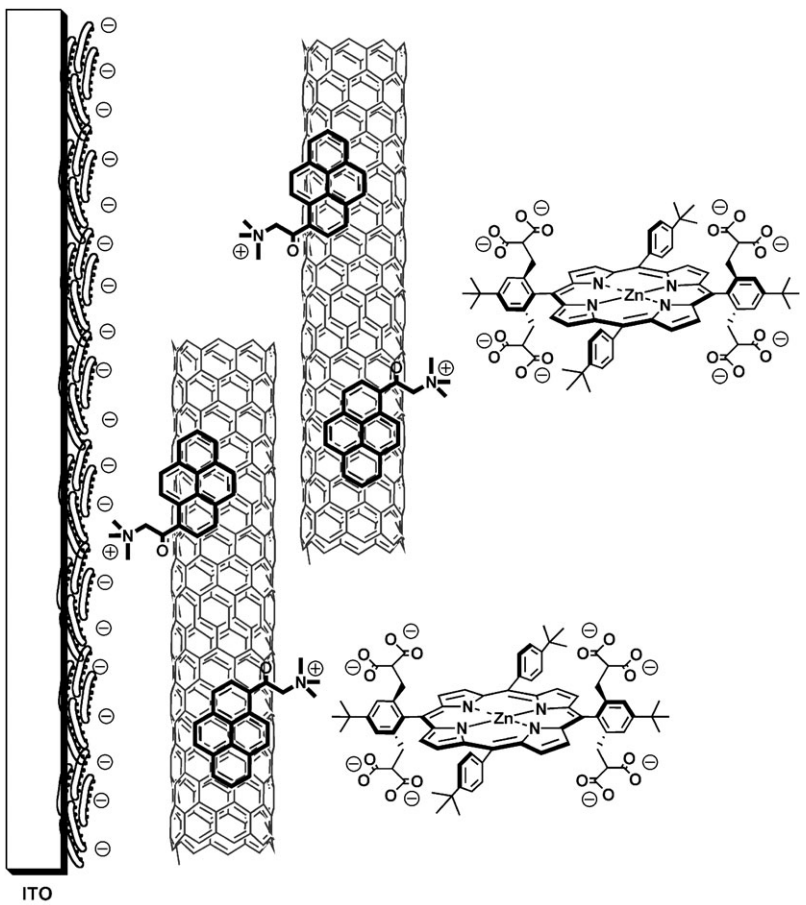

Scheme 20 Leading example of a SWNT/$pyrene^{+}$/ZnP^{8-} nanohybrid for photoelectrochemical cells.

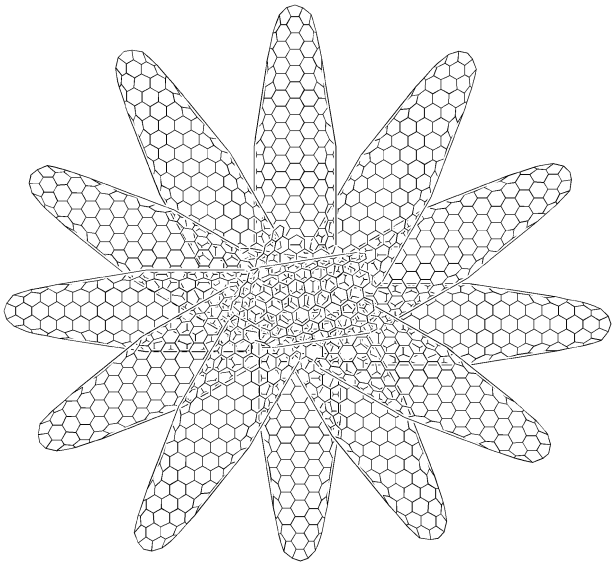

Scheme 21 Molecular building blocks—single wall carbon nanohorns (SWNH)—as electron acceptors.

to-photocurrent efficiency as high as 13% under an applied potential of 0.2 V *versus* SCE. The dual role of SWNT in promoting photoinduced charge separation and facilitating charge transport is presented.

Summary and outlook

In summary, combining nanometer scale carbon structures—fullerenes and carbon nanotubes—with electron donor groups represents an innovative concept to solar energy harvesting systems, which leads to appreciable conversion of solar light into practical electricity.[82]

In this context, the delocalization of charges—electrons or holes—within the giant, spherical carbon framework of fullerenes is of great interest. It offers unique opportunities for stabilizing charged entities. Unquestionably, the most striking observation is that charge recombination in ZnP–C_{60} and H_2P–C_{60} conjugates is located deep in the inverted region of the Marcus parabola, with lifetimes ranging from as short as tens of picoseconds to all the way to seconds. Please note that a time window of seconds is a time domain that has not been accomplished so far in artificial photosynthetic reaction centers.

Similarly, CNT (*i.e.*, SWNT and MWNT) have been combined with electron donors that lead to new generations of donor acceptor nanohybrids, which, upon illumination, give rise to slow charge recombination with lifetimes typically in the range of microseconds.

The lifetimes of the charge-separated species in most of the surveyed nanometer scale carbon structures are so long that these systems are excellent candidates for the fabrication of photovoltaic devices. In fact, in first attempts the photocurrents are quite high. It is reasonable to ascribe the limitations seen in the photocurrents to (i) the efficiency of electron–hole separation at the donor–acceptor interface or (ii) the efficiency of transfer of electrons from the electron acceptor to the electron collecting electrodes. Moreover, the efficiency of electron-hole separation might depend either on the inherent energy levels of the donor and the acceptor, or on the number and distance of contacts between the donor and the acceptor.

In terms of future prospects, particularly noteworthy are single wall carbon nanohorns (SWNH) see Scheme 21. These new nanometer scale carbon structures possess high porosity and large surface areas—Scheme 21.[81] SWNH are typically constituted by tubes of about 2–5 nm of diameter and 30 to 50 nm long, which associate with each other to give rise to round-shaped aggregates of 100 nm of diameter.

Acknowledgements

This work was carried out with partial support from the SFB 583, DFG (GU 517/4-1), FCI, and the Office of Basic Energy Sciences of the U.S. Department of Energy. I am deeply indebted to Profs. Ford, Fukuzumi, Hirsch, Imahori, Jux, Kotov, Maggini, Martin, Prato, Schuster, Sessler, Torres, Valli, and Zilbermann for their productive collaborations and numerous stimulating discussions. This Invited Article is dedicated to Professor Ortwin Brede on the occasion of his 65th birthday and his retirement.

References

1 *Basic Research Needs for Solar Energy Utilization*, Report of the Basic Energy Sciences Workshop on Solar Energy Utilization April 18–21, 2005—http://www.sc.doe.gov/bes/reports/files/SEU_rpt.pdf.
2 V. Balzani, *Electron Transfer in Chemistry*, Wiley-VCH, Weinheim, 2001, vol. I–V.
3 (*a*) A. Hirsch and M. Brettreich, *Fullerenes: Chemistry and Reactions*, Wiley-VCH, Weinheim, 2004; (*b*) K. M. Kadish and R. S. Ruoff, *Fullerenes: Chemistry, Physics, and Technology*, Wiley-VCH, Weinheim, 2000; (*c*) D. M. Guldi and N. Martin, *Fullerenes: From Synthesis to Optoelectronic Properties, Series: Developments in Fullerene Science*, Kluwer Academic, Dordrecht, 2002; (*d*) T. Braun, *Nuclear and Radiation Chemical Approaches to Fullerene Science Series: Developments in Fullerene Science*, Kluwer Academic, Dordrecht, 2000.
4 (*a*) F. Diederich, L. Isaacs and D. Philp, *Chem. Soc. Rev.*, 1994, **23**, 243; (*b*) M. Prato and M. Maggini, *Acc. Chem. Res.*, 1998, **31**, 519; (*c*) D. Tasis, N. Tagmatarchis, V. Georgakilas, C. Gamboz, M.-R. Soranzo and M. Prato, *Compt. Rend. Chim.*, 2003, **6**, 597; (*d*) N. Tagmatarchis and M. Prato, *Synlett*, 2003, **6**, 768; (*e*) F. Diederich and M. Gomez-Lopez, *Chem. Soc. Rev.*, 1999, **28**, 263.
5 (*a*) S. Reich, C. Thomsen and J. Maultzsch, *Carbon Nanotubes: Basic Concepts and Physical Properties*, Wiley-VCH, Weinheim, Germany, 2004; (*b*) M. S. Dresselhaus, G. Dresselhaus and P. Avouris, *Carbon Nanotubes: Synthesis, Structure, Properties and Applications*, Springer, Berlin, 2001; (*c*) P. J. F. Harris, *Carbon Nanotubes and Related Structures: New Materials for the Twenty-First Century*, Cambridge University Press, Cambridge, UK, 2001; (*d*) Special issue on Carbon Nanotubes, *Acc. Chem. Res.*, 2002, **35**, 997; (*e*) S. Roth and D. Carroll, *One-Dimensional Metals: Conjugated Polymers, Organic Crystals, Carbon Nanotubes*, Wiley-VCH, Weinheim, Germany, 2004; (*f*) V. N. Popov and P. Lambin, *Carbon Nanotubes*, Springer, Dordrecht, 2006.
6 (*a*) T. W. Ebbesen and P. M. Ajayan, *Nature*, 1992, **358**, 220; (*b*) S. Iijima and T. Ichihaschi, *Nature*, 1993, **364**, 737; (*c*) C. H. C. Bethune, M. S. de Vries, G. Gorman, R. Savoy, J. Vazques and R. Beyers, *Nature*, 1993, **363**, 605.
7 (*a*) Y. Zhang, T. Ichihashi, E. Landree, F. Nihey and S. Iijima, *Science*, 1999, **285**, 1719; (*b*) M. S. Gudiksen, L. J. Lauhon, J. Wang, D. C. Smith and C. M. Lieber, *Nature*, 2002, **415**, 617; (*c*) H. Dai, *Acc. Chem. Res.*, 2002, **35**, 1035; (*d*) J. J. Davis,

K. S. Coleman, B. R. Azamian, C. B. Bagshaw and M. L. H. Green, *Chem.–Eur. J.*, 2003, **9**, 3733; (*e*) G. G. Wildgoose, C. E. Banks, H. C. Leventis and R. G. Compton, *Microchim. Acta*, 2006, **152**, 187; (*f*) C. Hu, X. Chen and S. Hu, *J. Electroanal. Chem.*, 2006, **586**, 77; (*g*) J. J. Gooding, *Electrochim. Acta*, 2005, **50**, 3049; (*h*) E. Bekyarova, M. Davis, T. Burch, M. E. Itkis, B. Zhao, S. Sunshine and R. C. Haddon, *J. Phys. Chem. B*, 2004, **108**, 19717; (*i*) G. L. Luque, N. F. Ferreyra and G. A. Rivas, *Microchim. Acta*, 2006, **152**, 277; (*j*) P. W. Barone, S. Baik, D. A. Heller and M. S. Strano, *Nat. Mat.*, 2005, **4**, 86; (*k*) E. S. Snow, F. K. Perkins and J. A. Robinson, *Chem. Soc. Rev.*, 2006, **35**, 790; (*l*) P. Calvert, *Nature*, 1999, **399**, 210; (*m*) R. H. Baughman, A. A. Zakhidov and W. A. de Heer, *Science*, 2002, **297**, 787; (*n*) M. M. J. Treacy, T. W. Ebbesen and J. M. Gibson, *Nature*, 1996, **381**, 678; (*o*) B. Zhao, H. Hu, S. K. Mandal and R. C. Haddon, *Chem. Mater.*, 2005, **17**, 3235; (*p*) J. N. Coleman, U. Khan and Y. K. Gun'ko, *Adv. Mater.*, 2006, **18**, 689; (*q*) N. W. S. Kam, M. O'Connell, J. A. Wisdom and H. J. Dai, *Proc. Natl. Acad. Sci. U. S. A.*, 2005, **102**, 11600; (*r*) S. J. Son, J. Reichel, B. He, M. Schuchman and S. B. Lee, *J. Am. Chem. Soc.*, 2005, **127**, 7316; (*s*) C. R. Martin and P. Kohli, *Nat. Rev. Drug Discovery*, 2003, **2**, 29; (*t*) A. Bianco and M. Prato, *Adv. Mater.*, 2003, **15**, 1765; (*u*) A. Bianco, K. Kostarelos and M. Prato, *Curr. Opin. Chem. Biol.*, 2005, **9**, 674; (*v*) R. S. Ruoff and D. C. Lorents, *Carbon*, 1995, **33**, 925; (*w*) M. M. J. Treacy, T. W. Ebbesen and J. M. Gibson, *Nature*, 1996, **381**, 678; (*x*) M. R. Falvo, G. J. Clary, R. M. Taylor II, V. Chi, F. P. Brooks, Jr, S. Washburn and R. Superfine, *Nature*, 1997, **389**, 582; (*y*) S. G. Rao, L. Huang, W. Setyawan and S. Hong, *Nature*, 2003, **425**, 36.

8 A. Thess, R. Lee, P. Nikolaev, H. Dai, P. Petit, J. Robert, C. Xu, Y. H. Lee, S. G. Kim, A. G. Rinzler, D. T. Colbert, G. E. Scuseria, D. Tomanek, J. E. Fischer and R. E. Smalley, *Science*, 1996, **273**, 483.

9 (*a*) J. Li, Y. Zhang and M. Zhang, *Chem. Phys. Lett.*, 2002, **364**, 328; (*b*) M. Yoshida and J.-I. Aihara, *Phys. Chem. Chem. Phys.*, 1999, **1**, 227; (*c*) J.-I. Aihara and H. Kanno, *Chem. Phys. Lett.*, 2004, **398**, 440.

10 (*a*) K. Kalyanasundaram, *Photochemistry of Polypyridine and Porphyrin Complexes*, Academic Press, 1997; (*b*) M. Gouterman, P. M. Rentzepis and K. D. Straub, *Porphyrins: Excited States and Dynamics*, ACS Symposium Series, N° 321, 1987; (*c*) D. Dolphin, *The Porphyrins*, Academic Press, 1978; (*d*) K. M. Kadish, K. M. Smith and R. Guilard, *The Porphyrin Handbook*, Academic Press, 2003.

11 (*a*) R. A. Marcus and N. Sutin, *Biochim. Biophys. Acta*, 1985, **811**, 265; (*b*) R. A. Marcus, *Angew. Chem., Int. Ed. Engl.*, 1993, **32**, 1111.

12 (*a*) R. C. Haddon, *Acc. Chem. Res.*, 1988, **21**, 243; (*b*) R. C. Haddon, *Science*, 1993, **261**, 1545.

13 L. Echegoyen and L. E. Echegoyen, *Acc. Chem. Res.*, 1998, **31**, 593.

14 G. Duskesas and S. Larsson, *Theor. Chem. Acc.*, 1997, **97**, 110.

15 (*a*) D. M. Guldi and K.-D. Asmus, *J. Phys. Chem. A*, 1997, **101**, 1472; (*b*) D. M. Guldi and M. Prato, *Acc. Chem. Res.*, 2000, **33**, 695.

16 M. L. McGlashen, M. E. Blackwood and T. G. Spior, *J. Am. Chem. Soc.*, 1993, **115**, 2074.

17 R. C. Haddon, A. F. Hebard, M. J. Rosseinsky, D. W. Murphy, S. J. Duclos, K. B. Lyons, B. Miller, J. M. Rosamilia, R. M. Fleming, A. R. Kortan, S. H. Glarum, A. V. Makhija, A. J. Muller, R. H. Eick, S. M. Zahurak, R. Tycko, G. Dabbagh and F. A. Thiel, *Nature*, 1991, **350**, 320.

18 H. W. Kroto, J. R. Heath, S. C. O'Brien, S. F. Curl and R. E. Smalley, *Nature*, 1985, **318**, 162.

19 S. M. Bachilo, M. S. Strano, C. Kittrell, R. H. Hauge, R. E. Smalley and R. B. Weisman, *Science*, 2002, **298**, 2361.

20 M. S. Dresselaus, G. Dresselhaus, R. Saito and A. Jorio, *Phys. Rep.*, 2005, **409**, 47.

21 (*a*) N. Mataga, T. Asahi, Y. Kanda and T. Okada, *Chem. Phys.*, 1988, **127**, 249; (*b*) N. Mataga and H. Miyasaka, in *Electron Transfer from Isolated Molecules to Biomolecules Part 2*, ed. J. Jortner and M. Bixon, Wiley, New York, 1999; (*c*) N. Mataga, H. Chosrowjan, Y. Shibata, N. Yoshida, A. Osuka, T. Kikuzawa and T. Okada, *J. Am. Chem. Soc.*, 2001, **123**, 12422.

22 (*a*) D. M. Guldi and K. D. Asmus, *J. Am. Chem. Soc.*, 1997, **119**, 5744; (*b*) S. Fukuzumi, K. Ohkubo, H. Imahori and D. M. Guldi, *Chem.–Eur. J.*, 2003, **9**, 1585.

23 D. M. Guldi, P. Neta and K. D. Asmus, *J. Phys. Chem.*, 1994, **98**, 4617.

24 (*a*) M. E. El-Khouly, M. Fujitsuka and O. Ito, *J. Porphyrins Phthalocyanines*, 2000, **4**, 591; (*b*) J. Fujisawa, Y. Ohba and S. Yamauchi, *Chem. Phys. Lett.*, 1998, **282**, 181; (*c*) D. M. Martino and H. van Willigen, *J. Phys. Chem. A*, 2000, **104**, 10701.

25 T. Nojiri, M. M. Alam, H. Konami, A. Watanabe and O. Ito, *J. Phys. Chem. A*, 1997, **101**, 7943.

26 (*a*) E. Dietel, A. Hirsch, E. Eichborn, A. Rieker, S. Hackbarth and B. Röder, *Chem. Commun.*, 1998, 1981; (*b*) D. M. Guldi, C. Luo, M. Prato, E. Dietel and A. Hirsch, *Chem. Commun.*, 2000, 373; (*c*) D. M. Guldi, C. Luo, M. Prato, A. Troisi, F. Zerbetto, M. Scheloske, E. Dietel, W. Bauer and A. Hirsch, *J. Am. Chem. Soc.*, 2001, **123**, 9166.

27 N. Armaroli, G. Marconi, L. Echegoyen, J.-P. Bourgeois and F. Diederich, *Chem.–Eur. J.*, 2000, **6**, 1629.

28 (*a*) C. Luo, D. M. Guldi, H. Imahori, K. Tamaki and Y. Sakata, *J. Am. Chem. Soc.*, 2000, **122**, 6535; (*b*) H. Imahori, M. E. El-Khouly, M. Fujitsuka, O. Ito, Y. Sakata and S. Fukuzumi, *J. Phys. Chem. A*, 2001, **105**, 325; (*c*) H. Imahori, K. Tamaki, D. M. Guldi, C. Luo, M. Fujitsuka, O. Ito, Y. Sakata and S. Fukuzumi, *J. Am. Chem. Soc.*, 2001, **123**, 2607; (*d*) H. Imahori, N. V. Tkachenko, V. Vehmanen, K. Tamaki, H. Lemmetyinen, Y. Sakata and S. Fukuzumi, *J. Phys. Chem. A*, 2001, **105**, 1750.

29 (*a*) T. Drovetskaya, C. A. Reed and P. D. W. Boyd, *Tetrahedron Lett.*, 1995, **36**, 7971; (*b*) D. Kuciauskas, S. Lin, G. R. Seely, A. L. Moore, T. A. Moore, D. Gust, T. Drovetskaya, C. A. Reed and P. D. W. Boyd, *J. Phys. Chem.*, 1996, **100**, 15926.

30 A. Lembo, P. Tagliatesta and D. M. Guldi, *J. Phys. Chem. B*, 2006, **110**, 11424.

31 S. A. Vail, P. J. Krawczuk, D. M. Guldi, A. Palkar, L. Echegoyen, J. P. C. Tome, M. A. Fazio and D. I. Schuster, *Chem.–Eur. J.*, 2005, **11**, 3375.

32 H. Imahori, H. Yamada, D. M. Guldi, Y. Endo, A. Shimomura, S. Kundu, K. Yamada, T. Okada, Y. Sakata and S. Fukuzumi, *Angew. Chem., Int. Ed.*, 2002, **41**, 2344.

33 (*a*) H. Imahori, D. M. Guldi, K. Tamaki, Y. Yoshida, C. Luo, Y. Sakata and S. Fukuzumi, *J. Am. Chem. Soc.*, 2001, **123**, 6617; (*b*) D. M. Guldi, H. Imahori, K. Tamaki, Y. Kashiwagi, H. Yamada, Y. Sakata and S. Fukuzumi, *J. Phys. Chem. A*, 2004, **108**, 541; (*c*) C. Luo, D. M. Guldi, H. Imahori, K. Tamaki and Y. Sakata, *J. Am. Chem. Soc.*, 2000, **122**, 6535.

34 F. Giacalone, J. L. Segura, N. Martin, J. Ramey and D. M. Guldi, *Chem.–Eur. J.*, 2005, **11**, 4819.

35 Unpublished results.

36 (*a*) D. M. Guldi, A. Gouloumis, P. Vázquez and T. Torres, *Chem. Commun.*, 2002, 205; (*b*) D. M. Guldi, J. Ramey, M. Victoria Martínez-Díaz, A. de la Escosura, T. Torres and M. Prato, *Chem. Commun.*, 2002, 2774.

37 T. Nishioka, K. Tashiro, T. Aida, J.-Y. Zheng, K. Kinbara, K. Saigo, S. Sakamoto and K. Yamaguchi, *Macromolecules*, 2000, **33**, 9182.

38 H. Luo, M.-S. Choi, Y. Araki, O. Ito and T. Aida, *Bull. Chem. Soc.*, 2005, **78**, 405.

39 W.-S. Li, K. S. Kim, D.-L. Jiang, H. Tanaka, T. Kawai, J. H. Kwon, D. Kim and T. Aida, *J. Am. Chem. Soc.*, 2006, **128**, 10527.

40 H. Li, R. B. Martin, B. A. Harruff, R. A. Carino, L. F. Allard and Y.-P. Sun, *Adv. Mater.*, 2004, **16**, 896.

41 D. Baskaran, J. W. Mays, X. P. Zhang and M. S. Bratcher, *J. Am. Chem. Soc.*, 2005, **127**, 6916.

42 G. de la Torre, W. Blau and T. Torres, *Nanotechnology*, 2003, **14**, 765.

43 (*a*) M. Alvaro, P. Atienzar, P. de la Cruz, J. L. Delgado, H. Garcia and F. Langa, *J. Phys. Chem. B*, 2004, **108**, 12691; (*b*) M. Alvaro, P. Atienzar, P. de la Cruz, J. L. Delgardo, V. Troiani, H. Garcia, F. Langa, A. Palkar and L. Echegoyen, *J. Am. Chem. Soc.*, 2006, **128**, 6626.

44 F. Cheng and A. Adronov, *J. Am. Chem. Soc.*, 2006, **18**, 5389.

45 (*a*) S. Qin, D. Qin, W. T. Ford, J. E. Herrera, D. E. Resasco, S. M. Bachilo and R. B. Weisman, *Macromolecules*, 2004, **35**, 3965; (*b*) D. M. Guldi, G. M. A. Rahman, J. Ramey, M. Marcaccio,

D. Paolucci, F. Paolucci, S. Qin, W. T. Ford, D. Balbinot, N. Jux, N. Tagmatarchis and M. Prato, *Chem. Commun.*, 2004, 2034.
46 D. M. Guldi, G. M. A. Rahman, S. Qin, M. Tchoul, W. T. Ford, M. Marcaccio, D. Paolucci, F. Paolucci, S. Campidelli and M. Prato, *Chem.–Eur. J.*, 2006, **12**, 2152.
47 S. Campidelli, C. Sooambar, E. Lozano-Diz, C. Ehli, D. M. Guldi and M. Prato, *J. Am. Chem. Soc.*, 2006, **128**, 12544.
48 V. Georgakilas, F. Pellarini, M. Prato, D. M. Guldi, M. Melle-Franco and F. Zerbetto, *Proc. Natl. Acad. Sci. U. S. A.*, 2002, **99**, 5075.
49 D. M. Guldi, A. Gouloumis, P. Vazquez, T. Torres, V. Georgakilas and M. Prato, *J. Am. Chem. Soc.*, 2005, **127**, 5811.
50 (*a*) D. M. Guldi, Y. Tian, J. H. Fendler, H. Hungerbühler and K.-D. Asmus, *J. Phys. Chem.*, 1996, **100**, 2753; (*b*) Y. Tian, J. H. Fendler, H. Hungerbühler, D. M. Guldi and K.-D. Asmus, *Materials Science and Engineering, C*, 1999, **7**, 67.
51 D. M. Guldi, M. Maggini, S. Mondini, F. Guerin and J. H. Fendler, *Langmuir*, 2000, **16**, 1311.
52 (*a*) D. M. Guldi, C. Luo, D. Koktysh, N. A. Kotov, T. Da Ros, S. Bosi and M. Prato, *Nano Lett.*, 2002, **2**, 775; (*b*) D. M. Guldi, C. Luo, N. A. Kotov, T. Da Ros, S. Bosi and M. Prato, *J. Phys. Chem. B*, 2003, **107**, 7293.
53 D. M. Guldi, H. Taieb, G. M. A. Rahman, N. Tagmatarchis and M. Prato, *Adv. Mater.*, 2005, **17**, 871.
54 F. Cheng and A. Adronov, *Chem.–Eur. J.*, 2006, **12**, 5053.
55 F. Cheng, S. Zhang, A. Adronov, L. Echegoyen and F. Diederich, *Chem.–Eur. J.*, 2006, **12**, 6062.
56 (*a*) H. Murakami, T. Nomura and N. Nakashima, *Chem. Phys. Lett.*, 2003, **378**, 481; (*b*) G. M. A. Rahman, D. M. Guldi, S. Campidelli and M. Prato, *J. Mater. Chem.*, 2006, **16**, 62.
57 L. Cao, H.-Z. Chen, H. B. Zhou, L. Zhu, J.-Z. Sun, X.-B. Zhang, J.-M. Xu and M. Wang, *Adv. Mater.*, 2003, **15**, 909.
58 A. Satake, Y. Miyajima and Y. Kobuke, *Chem. Mater.*, 2005, **17**, 716.
59 J. Chen and C. P. Collier, *J. Phys. Chem. B*, 2005, **109**, 7605.
60 H. Li, B. Zhou, Y. Lin, L. Gu, W. Wang, K. A. S. Fernando, S. Kumar, L. F. Allard and Y.-P. Sun, *J. Am. Chem. Soc.*, 2004, **126**, 1014.
61 (*a*) D. M. Guldi, G. M. A. Rahman, N. Jux, N. Tagmatarchis and M. Prato, *Angew. Chem., Int. Ed.*, 2004, **43**, 5526; (*b*) C. Ehli, G. M. A. Rahman, N. Jux, D. Balbinot, D. M. Guldi, F. Paolucci, F. Marcaccio, D. Paolucci, M. Melle-Franco, F. Zerbetto, S. Campidelli and M. Prato, *J. Am. Chem. Soc.*, 2006, **128**, 11222.
62 D. M. Guldi, G. M. A. Rahman, N. Jux, D. Balbinot, N. Tagmatarchis and M. Prato, *Chem. Commun.*, 2005, 2038.
63 (*a*) D. M. Guldi and M. Prato, *Chem. Commun.*, 2004, 2517; (*b*) D. M. Guldi, G. M. A. Rahman, N. Jux, D. Balbinot, U. Hartnagel, N. Tagmatarchis and M. Prato, *J. Am. Chem. Soc.*, 2005, **127**, 9830.
64 (*a*) D. M. Guldi, *J. Phys. Chem. B*, 2005, **109**, 11432; (*b*) H. Imahori Y. Mori and Y. Matano, *J. Photochem. Photobiol. C: Photochem. Rev.*, 2003, **4**, 51; (*c*) H. Imahori, *Org. Biomol. Chem.*, 2004, **2**, 1425; (*d*) H. Imahori and S. Fukuzumi, *Adv. Mater.*, 2004, **14**, 525.
65 (*a*) C. Winder and N. S. Sariciftci, *J. Mater. Chem.*, 2004, **14**, 1077; (*b*) C. J. Brabec, N. S. Sariciftci and J. C. Hummelen, *Adv. Funct. Mater.*, 2001, **11**, 15.
66 M. A. Loi, P. Denk, H. Hoppe, H. Neugebauer, C. Winder, D. Meissner, C. Brabec, N. S. Sariciftci, A. Gouloumis, P. Vázquez and T. Torres, *J. Mater. Chem.*, 2003, **4**, 700.
67 A. Gouloumis, A. de la Escosura, P. Vazquez, T. Torres, A. Kahnt, D. M. Guldi, H. Neugebauer, C. Winder, M. Drees and N. S. Sariciftci, *Org. Lett.*, 2006, **8**, 5187.
68 A. de la Escosura, M. V. Martínez-Díaz, R. H. Grubbs, D. M. Guldi, T. Torres, H. Neugebauer and N. S. Sariciftci, *Chem. Asian J.*, 2006, **1**, 148.
69 (*a*) H. Imahori, H. Yamada, S. Ozawa, K. Ushida and Y. Sakata, *Chem. Commun.*, 1999, 1165; (*b*) H. Yamada, H. Imahori and S. Fukuzumi, *J. Mater. Chem.*, 2002, **12**, 2034.
70 H. Imahori, H. Norieda, H. Yamada, Y. Nishimura, I. Yamazaki, Y. Sakata and S. Fukuzumi, *J. Am. Chem. Soc.*, 2001, **123**, 100.
71 (*a*) H. Yamada, H. Imahori, Y. Nishimura, I. Yamazaki and S. Fukuzumi, *Adv. Mater.*, 2002, **14**, 892; (*b*) H. Yamada, H. Imahori, Y. Nishimura, I. Yamazaki, T. K. Ahn, S. K. Kim, D. Kim and S. Fukuzumi, *J. Am. Chem. Soc.*, 2003, **125**, 9129; (*c*) H. Imahori, M. Kimura, K. Hosomizu, T. Sato, T. K. Ahn, S. K. Kim, D. Kim, Y. Nishimura, I. Yamazaki, Y. Araki, O. Ito and S. Fukuzumi, *Chem.–Eur. J.*, 2004, **10**, 5111; (*d*) H. Yamada, H. Imahori, Y. Nishimura, I. Yamazaki, T. K. Ahn, S. K. Kim, D. Kim and S. Fukuzumi, *J. Am. Chem. Soc.*, 2003, **125**, 9129.
72 V. Chukharev, T. Vuorinen, A. Efimov, N. V. Tkachenko, M. Kimura, S. Fukuzumi, H. Imahori and H. Lemmetyinen, *Langmuir*, 2005, **21**, 6385.
73 Y. J. Cho, T. K. Ahn, H. Song, K. S. Kim, C. Y. Lee, W. S. Seo, K. Lee, S. K. Kim, D. Kim and J. T. Park, *J. Am. Chem. Soc.*, 2005, **127**, 2380.
74 (*a*) H. Imahori, J.-C. Liu, K. Hosomizu, T. Sato, Y. Mori, H. Hotta, Y. Matano, Y. Araki, O. Ito, N. Maruyama and S. Fujita, *Chem. Commun.*, 2004, 2066; (*b*) D. M. Guldi, I. Zilbermann, G. A. Anderson, K. Kordatos, M. Prato, R. Tafuro and L. Valli, *J. Mater. Chem.*, 2004, **14**, 303; (*c*) S. Conoci, D. M. Guldi, S. Nardis, R. Paolesse, K. Kordatos, M. Prato, G. Ricciardi, M. G. H. Vicente, I. Zilbermann and L. Valli, *Chem.–Eur. J.*, 2004, **10**, 6523; (*d*) T. Vuorinen, K. Kaunisto, N. V. Tkachenko, A. Efimov, H. Lemmetyinen, A. S. Alekseev, K. Hosomizu and H. Imahori, *Langmuir*, 2005, **21**, 5383; (*e*) D. M. Guldi, I. Zilbermann, G. Anderson, A. Li, D. Balbinot, N. Jux, M. Hatzimarinaki, A. Hirsch and M. Prato, *Chem. Commun.*, 2004, 726; (*f*) D. M. Guldi, F. Pellarini, M. Prato, C. Granito and L. Troisi, *Nano Lett.*, 2002, **2**, 965; (*g*) H. Imahori, J. C. Liu, H. Hotta, A. Kira, T. Umeyama, Y. Matano, G. Li, S. Ye, M. Isosomppi, N. V. Tkachenko and H. Lemmetyinen, *J. Phys. Chem. B*, 2005, **109**, 18465.
75 (*a*) T. Hasobe, H. Imahori, P. V. Kamat and S. Fukuzumi, *J. Am. Chem. Soc.*, 2003, **125**, 14962; (*b*) H. Imahori, A. Fujimoto, S. Kang, H. Hotta, K. Yoshida, T. Umeyama, Y. Matano and S. Isoda, *Adv. Mater.*, 2005, **17**, 1727; (*c*) T. Hasobe, H. Imahori, P. V. Kamat, T. K. Ahn, S. K. Kim, D. Kim, A. Fujimoto, T. Hirakawa and S. Fukuzumi, *J. Am. Chem. Soc.*, 2005, **127**, 1216.
76 T. Hasobe, P. V. Kamat, V. Troiani, N. Solladie, T. K. Ahn, S. K. Kim, D. Kim, A. Kongkanand, S. Kuwabata and S. Fukuzumi, *J. Phys. Chem. B*, 2005, **109**, 19.
77 (*a*) T. Hasobe, H. Imahori, S. Fukuzumi and P. V. Kamat, *J. Phys. Chem. B*, 2003, **107**, 12105; (*b*) T. Hasobe, P. V. Kamat, M. A. Absalom, Y. Kashiwagi, J. Sly, M. J. Crossley, K. Hosomizu, H. Imahori and S. Fukuzumi, *J. Phys. Chem. B*, 2004, **108**, 12865; (*c*) T. Hasobe, Y. Kashiwagi, M. A. Absalom, J. Sly, K. Hosomizu, M. J. Crossley, H. Imahori, P. V. Kamat and S. Fukuzumi, *Adv. Mater.*, 2004, **16**, 975; (*d*) H. Imahori, T. Hasobe, H. Yamada, P. V. Kamat, S. Barazzouk, M. Fujitsuka, O. Ito and S. Fukuzumi, *Chem. Lett.*, 2001, **8**, 784.
78 (*a*) D. M. Guldi, G. M. A. Rahman, M. Prato, N. Jux, S. Qin and W. T. Ford, *Angew. Chem., Int. Ed.*, 2005, **44**, 2015; (*b*) D. M. Guldi, G. M. A. Rahman, V. Sgobba, S. Campidelli and M. Prato, *Adv. Mater.*, 2006, **18**, 2264.
79 (*a*) D. M. Guldi, G. M. A. Rahman, V. Sgobba, N. A. Kotov, D. Bonifazi and M. Prato, *J. Am. Chem. Soc.*, 2006, **128**, 2315; (*b*) G. M. A. Rahman, D. M. Guldi, R. Cagnoli, A. Mucci, L. Schenetti, L. Vaccari and M. Prato, *J. Am. Chem. Soc.*, 2005, **127**, 10051.
80 T. Hasobe, S. Fukuzumi and P. V. Kamat, *J. Phys. Chem. B*, 2006, **110**, 25477.
81 G. Pagona, A. S. D. Sandanayaka, Y. Araki, J. Fan, N. Tagmatarchis, M. Yudasaka, S. Iijima and O. Ito, *J. Phys. Chem. B*, 2006, **110**, 20729.
82 N. Martín, *Chem. Commun.*, 2006, 2093.

